Title: Two stage evolution of mammalian ==adipose tissue== thermogenesis

Authors: Susanne Keipert[1†], Michael J. Gaudry[1†], Maria Kutschke[1], ==Michaela Keuper[1], Margeoux A.S. Dela Rosa[2]==, Yiming Cheng[3], José M. Monroy Kuhn[4], Rutger Laterveer[1], Camila A. Cotrim[2], Peter Giere[5], Fabiana Perocchi[3], ==Regina Feederle[6]==, Paul G. Crichton[2], Dominik Lutter[4], Martin Jastroch[1*]

Affiliations:

[1]Department of Molecular Biosciences, The Wenner-Gren Institute, Stockholm University, SE-106 91, Stockholm, Sweden.

[2]Biomedical Research Centre, Norwich Medical School, University of East Anglia, Norwich Research Park, Norwich, NR4 7TJ, United Kingdom

[3]Institute of Neuronal Cell Biology, Technical University of Munich, Biedersteiner Straße 29, 80802 Munich, Germany; Munich Cluster of Systems Neurology, Feodor-Lynen-Straße 17, 81377 Munich, Germany; Institute for Diabetes and Obesity, Helmholtz Zentrum München, Ingolstädter Landstraße 1, 85764 Munich, Germany

[4]Computational Discovery Research, Institute for Diabetes and Obesity (IDO), Helmholtz Diabetes Center (HDC), Helmholtz Zentrum Munich - German Research Center for Environmental Health; German Center for Diabetes Research (DZD), 85764 Neuherberg, Germany

[5]Museum für Naturkunde, Leibniz Institute for Evolution and Biodiversity Science, Berlin, Germany

[6]Monoclonal Antibody Core Facility, Helmholtz Zentrum München, German Research Center for Environmental Health, 85764 Neuherberg, Germany.

5

† These authors contributed equally to this work

*Corresponding author. Email: martin.jastroch@su.se

Abstract: Brown adipose tissue (BAT) is a heater organ that expresses thermogenic uncoupling

10   protein 1 (UCP1) to maintain high body temperatures during cold stress. BAT thermogenesis is

considered an overarching mammalian trait but its evolutionary origin is unknown. We show that

adipose tissue of marsupials, which diverged from eutherian mammals ~150 million years ago,

expresses a non-thermogenic UCP1 variant governed by a partial transcriptomic BAT signature

that is similar to that found in eutherian beige adipose tissue. We found that the reconstructed

15   UCP1 sequence of the common eutherian ancestor displayed typical thermogenic activity, while

therian ancestor UCP1 is non-thermogenic. Thus, mammalian adipose tissue thermogenesis may

have evolved in two distinct stages, with a pre-thermogenic stage in the common therian ancestor

linking UCP1 expression to adipose tissue and thermal stress. We proposed that in a second stage,

UCP1 acquired its thermogenic function specifically in eutherians, such that the onset of

20   mammalian BAT thermogenesis occurred only after the divergence from marsupials.

One-Sentence Summary: Evidence that UCP1 thermogenesis evolved in eutherian mammals,
underlying their successful radiation into cold climates.

Main text

The evolution of thermogenesis in mammals supported the maintenance of high body temperatures, which came with the benefits of climate-independent motility and reproduction, increased brain size and regulation of growth and body weight. In particular brown adipose tissue (BAT), the main organ for non-shivering thermogenesis in mammals, enables newborn, small-sized species and hibernators to increase heat output to overcome cold stress. Critical for BAT thermogenesis is the expression of the uncoupling protein 1 (UCP1), which resides in the inner mitochondrial membrane. Free fatty acids, liberated by cold- or diet-stimulated lipolysis, induce proton transport by UCP1 to uncouple the respiratory chain from ATP production to accelerate metabolism and release more chemical energy as heat (*1*). Although BAT has been labelled a 'mammalian prerogative' (*2*), experimental studies on BAT and UCP1 function are limited to only a few eutherian species, mostly rodents and humans. In particular investigations in humans have been fostered by the identification of functional BAT in adults (*3–5*) which represents a promising therapeutic target to combat metabolic diseases such as obesity and cardiovascular complications by increasing energy metabolism (*6*). In white adipose tissue (WAT) of mice and humans, cells with partial BAT features, termed beige adipocytes, can emerge under stress conditions, but their physiological role is still a matter of debate (*7, 8*). Pharmacologic and genetic manipulations in mice have been used to understand how BAT thermogenesis can be activated, brown adipocytes recruited, or white adipocytes transformed into beige cells. The structure of human UCP1 has been determined (*9, 10*), but the mechanism of proton transport, which is pivotal for thermogenesis, has remained enigmatic.

As revealed by comparative genomics, the UCP1 gene is ancient, dating back to the divergence of teleosts (ray-finned fish) and sarcopterygians (lobe-finned fish) about 420 million years ago

(*11*). In fish, UCP1 is expressed in liver and brain tissues, but not in adipocytes, raising questions surrounding the evolutionary timing of targeted UCP1 expression in adipocyte-like cells, as in mice and humans. Furthermore, the protein function of the fish UCP1 orthologue is unknown and phylogenetic inference shows its sequence to be quite similar to that of its paralogues UCP2 and UCP3. Apart from mammalian UCP1 variants, all other members of the mitochondrial solute carrier family SLC25 are metabolite transporters (*12*, *13*). Even UCP2 and UCP3, previously thought to be alternative thermogenic protonophores, have no physiological role in thermogenesis (*14*) but appear to transport small metabolites (*12*). The demonstration of BAT thermogenesis in an afrotherian species, the lesser-hedgehog tenrec (*Echinops telfairi*), revealed that UCP1 has acquired its heat-producing role prior to the divergence of afrotherian and boreoeutherian mammals about 80 million years ago (*15*). The role of UCP1 in marsupials, which diverged from eutherians about 120-180 million years ago, is less clear. Marsupials possess a UCP1 orthologue (*16*), but *in vivo* evidence for adaptive non-shivering thermogenesis has remained equivocal (reviewed by (*17*)).

We discovered a gene expression signature of UCP1-expressing adipose tissue in marsupials with global transcriptomic methods that is reminiscent of eutherian beige adipose tissue. We then assessed the thermogenic capacity of marsupial UCP1 and resurrected the reconstructed UCP1 sequence of the common eutherian and therian ancestors for functional analyses to pinpoint the origin of UCP1-dependent thermogenesis.

Results

Development of endothermy and UCP1 expression in the opossum

To compare the transcriptomes of marsupial and eutherian adipose tissue, we scrutinized the short-tailed opossum, *Monodelphis domestica*, a marsupial model organism with high genomic

sequencing coverage. Offspring of *M. domestica* develop predominantly *ex utero*, are hairless and initially ectothermic, receiving body heat from the mother (Fig. 1A). The young were investigated during, and shortly after weaning at ages of 6 to 13 weeks at which point they experience thermal stress, and during adulthood at 33 weeks (Fig. 1B). Body weight, length, blood markers and the appearance of adipose tissue were recorded during development (Fig. 1C and D, S1A and B). Infrared thermography of eye temperatures revealed that 6-week old juveniles separated from their mothers were unable to maintain the nursing temperature of about 32°C, in contrast to the sustained endothermic homeothermy of ≥8-weeks individuals (Fig. 1E). Body temperatures were confirmed by rectal probing (Fig. 1F), consistent with reports on the development of thermoregulatory competence in marsupials (*18*, *19*). UCP1 mRNA expression was exclusively found in adipose tissue depots (Fig. 1G) with amounts transiently increasing from age 6 to 10 weeks (Fig. 1H), coinciding with the onset of sustained endothermy. UCP1 mRNA expression was lower in the interscapular adipose tissue (AT), the canonical location of eutherian BAT, than in the inguinal AT, which is a prominent site for the occurrence of beige adipocytes in eutherian mammals. In the anterior subcutaneous AT, UCP1 was barely detectable throughout juvenile development (Fig. 1H).

Comparative transcriptomics reveal a partial browning signature in the opossum

We attempted to understand the underlying molecular network governing marsupial UCP1 expression by determining the global transcriptomic changes of 6-week old (low UCP1) vs. 10-week old (high UCP1) opossums. Comparative analyses to cold-induced changes in mouse BAT served to identify common or divergent features between marsupial and eutherian adipose tissue. Plotting the whole cold-induced mouse BAT transcriptome (y-axis) against the marsupial transcriptome (x-axis) depicted common significant gene expression changes (purple dots, Fig.

2A). The overlap or enrichment of significantly regulated genes (squares) was significantly higher than expected in all intersections between mouse BAT and opossum inguinal AT (all p< 0.001), but not between mouse BAT and interscapular AT or anterior subcutaneous AT. Thus, opossum inguinal AT displayed a gene regulation network similar to that in cold-activated mouse BAT.

5 Expression of beta3-adrenergic receptor mRNA, which predominantly mediates the thermogenic response in eutherian BAT, was increased specifically in opossum inguinal AT, whereas abundance of the beta 1-receptor mRNA was increased in all adipose depots (Fig. 2B). Of potential UCP1-independent thermogenic pathways, the opossum shows increased expression only of creatine kinase B (ckb) (Fig. S2A), implicated in an ATP-dependent thermogenic futile creatine

10 cycle (20), but no alterations in Alpl, Serca2B or any ATP-synthase subunits (Fig. S2B). Differentially expressed genes (DEGs) of marsupial inguinal AT between 6-week and 10-week old animals were compared to those of interscapular, anterior subcutaneous AT, mouse BAT and WAT. The heat map depicts that expression patterns in all adipose tissue depots of 6-week old opossums resemble that in mouse WAT (Fig. 2C). A molecular network was observed in marsupial

15 inguinal AT at 10 weeks of age that resembled that of mouse BAT. The mouse BAT-like expression pattern of these genes is less pronounced in interscapular AT and absent in the anterior subcutaneous depot (Fig. 2C). A stringent BAT signature based on mouse and human transcriptomes was used to approximate the degree of browning from white to beige to brown AT (21). The reference mouse transcriptome of BAT exhibited full browning irrespective of

20 acclimation temperature (Fig. 2D), whereas mouse inguinal AT shows a partial browning signature in the cold, characteristic of beige adipocytes with induced UCP1 expression (7, 22). The opossum ATs enhance the browning probability alongside increased UCP1 expression from 6 to 10 weeks of age, particularly in inguinal AT. However, none of the individuals displayed a pure BAT-specific molecular signature, which is represented by a probability of 1.0, depicted as fully

browned bar (Fig. 2D). Thus, marsupial adipose tissue appears to regulate UCP1 in a molecular network that is reminiscent of that proposed to occur in eutherian beige adipose tissue.

Comparative respirometry demonstrates lack of thermogenic function of marsupial UCP1

We investigated marsupial UCP1 function by overexpressing mouse and opossum UCP1 in human embryonic kidney HEK293 cells, an established mammalian test system (*23, 24*) (Fig. 3A). UCP1 mRNA expression was similar between mouse (Mm UCP1) and opossum UCP1 (Md UCP1) (Fig. S3A). Among commercially available mouse UCP1 antibodies, only one detected opossum UCP1 weakly, prompting us to generate a strong, specific opossum UCP1 antibody and protein standards of mouse and opossum UCP1 for the immunoblot quantification as described previously (*15*) (Fig. S3B and C). Protein standards and the specific antibodies enabled us to quantify the UCP1 protein levels of low and high mouse UCP1-expressing clones (Fig. 3B, S3D, F and H) and opossum UCP1-expressing clones (Fig. 3C, S3E, G and H). We applied plate-based respirometry of intact HEK293 cells to measure UCP1-dependent proton leak upon stimulation with a naturally-occurring activators such as the long-chain fatty acid palmitate and the short-chain fatty acid nonanoic acid, as well as the more recently identified artificial activator Arotinoid acid, a retinoic acid analogue (commonly referred to as TTNPB) (*25*) (Fig. 3D). Palmitate, TTNPB and nonanoic acids activated proton leak specifically in cells expressing low and high levels of mouse UCP1, but not in cells expressing high levels of opossum UCP1 or empty vector controls (Fig. 3E-I). Additionally, no proton transport activity was found in a non-clonal mixture of transiently transfected opossum UCP1 cells (Fig. S3H and I). In isolated mitochondria, mouse UCP1 was activatable with nonanoic acids and fully inhibitable with its canonical inhibitor, guanosine diphosphate, as judged by decreases in mitochondrial membrane potential measured with the fluorometric indicator safranin O. By contrast, neither basal protonophoric activity, nor activation

or inhibition was observed for opossum UCP1 (Fig. 3J, S3J). Thus, opossum UCP1 is not thermogenic and typical thermogenic features must have been either introduced at later evolutionary stages or lost in the opossum lineage. Opossum UCP1 displays 65 dissimilar (in dark blue) and 46 similar (light blue) amino acids as compared to mouse UCP1 (Fig. 3K), which may reflect changes during the course of evolution that introduced strictly regulated activation and inhibition of UCP1 for regulation of adaptive thermogenic function.

Reconstruction and functional analysis of the stem eutherian and therian ancestor UCP1

To pinpoint the phylogenetic origin of thermogenic UCP1, we collected and verified 237 intact mammalian UCP1 sequences (Table S2), excluding the inactive versions (*26*). We applied a maximum likelihood and phylogenetic approach to reconstruct the predicted ancestral UCP1 sequences of the major nodes of the mammalian phylogenetic tree (Fig. S4, Table S2 and S3), such as UCP1 from the stem eutherian ancestor (Fig. 4A). Next, we synthetized the stem eutherian UCP1 sequence (Fig. S4 node 6), controlled for mRNA expression and protein levels (Fig. S5A and B) and tested its function (Fig. 4B, S5C). Proton transport activity of the reconstructed ancient eutherian UCP1 protein was activatable with TTNPB (Fig. 4B and C) and nonanoic acids (Fig. S5C), as is eutherian UCP1 of extant species. Thus, we proposed that the thermogenic function of eutherian UCP1 may have occurred before the radiation of eutherian mammals, which was around 65-100 million years ago (*27, 28*). To exclude that marsupials have specifically lost thermogenic UCP1 function, we transiently transfected the reconstructed stem therian UCP1 (Fig. S4, node 8), which appeared to share more similar amino acid residues with opossum than with the stem eutherian UCP1 (Fig. 4D). Protein levels of opossum and therian UCP1 were similar (Fig. 4E) and comparable to previous experiments (Fig. S3H). The therian version was not activatable by palmitate or TTNPB (Fig. 4F), similar to opossum UCP1. Thus, good arguments can be put

forward that the acquisition of thermogenic function occurred after the divergence of marsupials. The acquired thermogenic features of eutherian UCP1 appear to reside within amino acid residues which are distinct from the marsupial and reconstructed stem therian UCP1 sequence (Fig. 4D). UCPs are members of the mitochondrial carrier family of solute transporters and conserve key structural features to support function (*29*, *30*) (Fig. 4G ; S6). Notably, we identified that the predicted cytoplasmic bonding network of UCP1 that gates access to the central cavity from the cytoplasmic side in all eutherian UCP1 variants is distinct from the stronger network found in all marsupials and monotremes (Fig. S7), the reconstructed stem therian UCP1 and mammalian UCP2 and UCP3 (*29*, *30*) (Fig 4H).

Discussion

The evolutionary origin of thermogenic eutherian BAT has been debated and molecular clues on the evolutionary events incorporating thermogenesis into adipose tissue have been lacking. Our data demonstrate that thermogenic adipose tissue appears to have evolved in two stages, with an initial pre-thermogenic stage in which UCP1 expression occurred in adipose tissue and coincided with weaning when juveniles experience cold stress, with pathways under adrenergic stimulation, possibly enabling mobilization of fat stores and other metabolic pathways. In a second stage, we propose gain of thermogenic function of a mitochondrial transporter, UCP1, enabled mitochondrial proton transport that is required to convert energy to heat.

BAT-like transcriptional control of marsupial UCP1 existed prior to the divergence of Marsupialia about 120-180 MYA, given exclusive UCP1 mRNA expression in adipose tissue with highest amounts detected during juvenile development of sustained endothermy, identical to what is found in most eutherians. The presence of a partial BAT transcriptomic signature is more reminiscent of that in eutherian beige than brown adipose tissue. In contrast to eutherian BAT, marsupial proto-

BAT or beige adipose tissue appears not to be thermogenic, as indicated by the lack of protonophoric activity of marsupial UCP1.

Like those of many of the ~50 different mitochondrial carriers present in mammals, the molecular function of pre-thermogenic marsupial UCP1 is unknown. The key structural features important for carrier function are well-conserved across the UCP sub-family. However, the important cytoplasmic bonding network for instance, gating the central cavity from the mitochondrial intermembrane space, (*9*, *10*, *31*) is identical between marsupial and therian UCP1, and mammalian UCP2 and UCP3, while eutherian UCP1 has distinctions that potentially contribute to its protonophoric activity (Fig. 4H). Other conserved residues, for example the eutherian UCP1 specific glutamate in position 134 was implicated in proton transport by some (*32*) but not by others (*33*). Given the similarity of marsupial UCP1 to non-thermogenic UCP2 and UCP3 (*14*), a conventional metabolite transport function is the likely function of UCP1 in non-eutherians (*12*, *31*).

References and Notes

1. D. G. Nicholls, R. M. Locke, Thermogenic mechanisms in brown fat. *Physiol Rev* **64**, 1–64 (1984).

2. B. Cannon, J. Nedergaard, Brown Adipose Tissue: Function and Physiological Significance. *Physiological Reviews* **84**, 277–359 (2004).

3. A. M. Cypess, S. Lehman, G. Williams, I. Tal, D. Rodman, A. B. Goldfine, F. C. Kuo, E. L. Palmer, Y.-H. Tseng, A. Doria, G. M. Kolodny, C. R. Kahn, Identification and Importance of Brown Adipose Tissue in Adult Humans. *N Engl J Med* **360**, 1509–1517 (2009).

4. W. D. van Marken Lichtenbelt, J. W. Vanhommerig, N. M. Smulders, J. M. A. F. L. Drossaerts, G. J. Kemerink, N. D. Bouvy, P. Schrauwen, G. J. J. Teule, Cold-Activated Brown Adipose Tissue in Healthy Men. *N Engl J Med* **360**, 1500–1508 (2009).

5. K. A. Virtanen, M. E. Lidell, J. Orava, M. Heglind, R. Westergren, T. Niemi, M. Taittonen, J. Laine, N.-J. Savisto, S. Enerbäck, P. Nuutila, Functional Brown Adipose Tissue in Healthy Adults. *N Engl J Med* **360**, 1518–1525 (2009).

6.   T. Becher, S. Palanisamy, D. J. Kramer, M. Eljalby, S. J. Marx, A. G. Wibmer, S. D. Butler, C. S. Jiang, R. Vaughan, H. Schöder, A. Mark, P. Cohen, Brown adipose tissue is associated with cardiometabolic health. *Nat Med* **27**, 58–65 (2021).

7.   J. Wu, P. Boström, L. M. Sparks, L. Ye, J. H. Choi, A.-H. Giang, M. Khandekar, K. A. Virtanen, P. Nuutila, G. Schaart, K. Huang, H. Tu, W. D. van Marken Lichtenbelt, J. Hoeks, S. Enerbäck, P. Schrauwen, B. M. Spiegelman, Beige Adipocytes Are a Distinct Type of Thermogenic Fat Cell in Mouse and Human. *Cell* **150**, 366–376 (2012).

8.   S. Keipert, M. Jastroch, Brite/beige fat and UCP1 — is it thermogenesis? *Biochimica et Biophysica Acta (BBA) - Bioenergetics* **1837**, 1075–1082 (2014).

9.   S. A. Jones, P. Gogoi, J. J. Ruprecht, M. S. King, Y. Lee, T. Zögg, E. Pardon, D. Chand, S. Steimle, D. M. Copeman, C. A. Cotrim, J. Steyaert, P. G. Crichton, V. Moiseenkova-Bell, E. R. S. Kunji, Structural basis of purine nucleotide inhibition of human uncoupling protein 1. *Science Advances* **9**, eadh4251 (2023).

10. Y. Kang, L. Chen, Structural basis for the binding of DNP and purine nucleotides onto UCP1. *Nature*, 1–2 (2023).

11. M. Jastroch, S. Wuertz, W. Kloas, M. Klingenspor, Uncoupling protein 1 in fish uncovers an ancient evolutionary history of mammalian nonshivering thermogenesis. *Physiol Genomics* **22**, 150–156 (2005).

12. A. Vozza, G. Parisi, F. De Leonardis, F. M. Lasorsa, A. Castegna, D. Amorese, R. Marmo, V. M. Calcagnile, L. Palmieri, D. Ricquier, E. Paradies, P. Scarcia, F. Palmieri, F. Bouillaud, G. Fiermonte, UCP2 transports C4 metabolites out of mitochondria, regulating glucose and glutamine oxidation. *Proc Natl Acad Sci U S A* **111**, 960–965 (2014).

13. F. Palmieri, The mitochondrial transporter family (SLC25): physiological and pathological implications. *Pflugers Arch* **447**, 689–709 (2004).

14. J. Nedergaard, B. Cannon, The 'Novel''Uncoupling' Proteins UCP2 and UCP3: What Do They Really do? Pros and Cons for Suggested Functions. *Experimental Physiology* **88**, 65–84 (2003).

15. R. Oelkrug, N. Goetze, C. Exner, Y. Lee, G. K. Ganjam, M. Kutschke, S. Müller, S. Stöhr, M. H. Tschöp, P. G. Crichton, G. Heldmaier, M. Jastroch, C. W. Meyer, Brown fat in a protoendothermic mammal fuels eutherian evolution. *Nat Commun* **4**, 2140 (2013).

16. M. Jastroch, K. W. Withers, S. Taudien, P. B. Frappell, M. Helwig, T. Fromme, V. Hirschberg, G. Heldmaier, B. M. McAllan, B. T. Firth, T. Burmester, M. Platzer, M. Klingenspor, Marsupial uncoupling protein 1 sheds light on the evolution of mammalian nonshivering thermogenesis. *Physiol Genomics* **32**, 161–169 (2008).

17. M. Jastroch, E. T. Polymeropoulos, M. J. Gaudry, Pros and cons for the evidence of adaptive non-shivering thermogenesis in marsupials. *J Comp Physiol B* **191**, 1085–1095 (2021).

18. P. Morrison, J. H. Petajan, The Development of Temperature Regulation in the Opossum, Didelphis marsupialis virginiana. *Physiological Zoology* **35**, 52–65 (1962).

19. F. Geiser, L. Matwiejczyk, R. V. Baudinette, From Ectothermy to Heterothermy: The Energetics of the Kowari, Dasyuroides byrnei (Marsupialia: Dasyuridae). *Physiological Zoology* **59**, 220–229 (1986).

20. J. F. Rahbani, A. Roesler, M. F. Hussain, B. Samborska, C. B. Dykstra, L. Tsai, M. P. Jedrychowski, L. Vergnes, K. Reue, B. M. Spiegelman, L. Kazak, Creatine kinase B controls futile creatine cycling in thermogenic fat. *Nature* **590**, 480–485 (2021).

21. Y. Cheng, L. Jiang, S. Keipert, S. Zhang, A. Hauser, E. Graf, T. Strom, M. Tschöp, M. Jastroch, F. Perocchi, Prediction of Adipose Browning Capacity by Systematic Integration of Transcriptional Profiles. *Cell Rep* **23**, 3112–3125 (2018).

22. J. M. A. de Jong, W. Sun, N. D. Pires, A. Frontini, M. Balaz, N. Z. Jespersen, A. Feizi, K. Petrovic, A. W. Fischer, M. H. Bokhari, T. Niemi, P. Nuutila, S. Cinti, S. Nielsen, C. Scheele, K. Virtanen, B. Cannon, J. Nedergaard, C. Wolfrum, N. Petrovic, Human brown adipose tissue is phenocopied by classical brown adipose tissue in physiologically humanized mice. *Nat Metab* **1**, 830–843 (2019).

23. M. Jastroch, V. Hirschberg, M. Klingenspor, Functional characterization of UCP1 in mammalian HEK293 cells excludes mitochondrial uncoupling artefacts and reveals no contribution to basal proton leak. *Biochim Biophys Acta* **1817**, 1660–1670 (2012).

24. M. J. Gaudry, M. Jastroch, Comparative functional analyses of UCP1 to unravel evolution, ecophysiology and mechanisms of mammalian thermogenesis. *Comparative Biochemistry and Physiology Part B: Biochemistry and Molecular Biology* **255**, 110613 (2021).

25. P. Tomás, J. Jiménez-Jiménez, P. Zaragoza, V. Vuligonda, R. A. S. Chandraratna, E. Rial, Activation by retinoids of the uncoupling protein UCP1. *Biochimica et Biophysica Acta (BBA) - Bioenergetics* **1658**, 157–164 (2004).

26. M. J. Gaudry, M. Jastroch, J. R. Treberg, M. Hofreiter, J. L. A. Paijmans, J. Starrett, N. Wales, A. V. Signore, M. S. Springer, K. L. Campbell, Inactivation of thermogenic UCP1 as a historical contingency in multiple placental mammal clades. *Sci Adv* **3**, e1602878 (2017).

27. R. W. Meredith, J. E. Janečka, J. Gatesy, O. A. Ryder, C. A. Fisher, E. C. Teeling, A. Goodbla, E. Eizirik, T. L. L. Simão, T. Stadler, D. L. Rabosky, R. L. Honeycutt, J. J. Flynn, C. M. Ingram, C. Steiner, T. L. Williams, T. J. Robinson, A. Burk-Herrick, M. Westerman, N. A. Ayoub, M. S. Springer, W. J. Murphy, Impacts of the Cretaceous Terrestrial Revolution and KPg extinction on mammal diversification. *Science* **334**, 521–524 (2011).

28. M. A. O'Leary, J. I. Bloch, J. J. Flynn, T. J. Gaudin, A. Giallombardo, N. P. Giannini, S. L. Goldberg, B. P. Kraatz, Z.-X. Luo, J. Meng, X. Ni, M. J. Novacek, F. A. Perini, Z. S. Randall, G. W. Rougier, E. J. Sargis, M. T. Silcox, N. B. Simmons, M. Spaulding, P. M. Velazco, M. Weksler, J. R. Wible, A. L. Cirranello, The placental mammal ancestor and the post-K-Pg radiation of placentals. *Science* **339**, 662–667 (2013).

29. J. J. Ruprecht, E. R. S. Kunji, The SLC25 Mitochondrial Carrier Family: Structure and Mechanism. *Trends Biochem Sci* **45**, 244–258 (2020).

30. J. J. Ruprecht, M. S. King, T. Zögg, A. A. Aleksandrova, E. Pardon, P. G. Crichton, J. Steyaert, E. R. S. Kunji, The Molecular Mechanism of Transport by the Mitochondrial ADP/ATP Carrier. *Cell* **176**, 435-447.e15 (2019).

31. A. J. Robinson, C. Overy, E. R. S. Kunji, The mechanism of transport by mitochondrial carriers based on analysis of symmetry. *Proc Natl Acad Sci U S A* **105**, 17766–17771 (2008).

32. J. Jiménez-Jiménez, R. Zardoya, A. Ledesma, M. García de Lacoba, P. Zaragoza, M. Mar González-Barroso, E. Rial, Evolutionarily Distinct Residues in the Uncoupling Protein UCP1 Are Essential for Its Characteristic Basal Proton Conductance. *Journal of Molecular Biology* **359**, 1010–1022 (2006).

33. M. Klingenberg, K. S. Echtay, M. Bienengraeber, E. Winkler, S. G. Huang, Structure–Function Relationship in UCP1. *Int J Obes* **23**, S24–S29 (1999).

34. A. Dobin, C. A. Davis, F. Schlesinger, J. Drenkow, C. Zaleski, S. Jha, P. Batut, M. Chaisson, T. R. Gingeras, STAR: ultrafast universal RNA-seq aligner. *Bioinformatics* **29**, 15–21 (2013).

35. M. I. Love, W. Huber, S. Anders, Moderated estimation of fold change and dispersion for RNA-seq data with DESeq2. *Genome Biology* **15**, 550 (2014).

36. M. E. Ritchie, B. Phipson, D. Wu, Y. Hu, C. W. Law, W. Shi, G. K. Smyth, limma powers differential expression analyses for RNA-sequencing and microarray studies. *Nucleic Acids Res* **43**, e47 (2015).

37. L. Xu, Z. Dong, L. Fang, Y. Luo, Z. Wei, H. Guo, G. Zhang, Y. Q. Gu, D. Coleman-Derr, Q. Xia, Y. Wang, OrthoVenn2: a web server for whole-genome comparison and annotation of orthologous clusters across multiple species. *Nucleic Acids Res* **47**, W52–W58 (2019).

38. R. C. Edgar, MUSCLE: multiple sequence alignment with high accuracy and high throughput. *Nucleic Acids Res* **32**, 1792–1797 (2004).

39. Z. Yang, PAML 4: phylogenetic analysis by maximum likelihood. *Mol Biol Evol* **24**, 1586–1591 (2007).

40. J. A. Stuart, J. A. Harper, K. M. Brindle, M. B. Jekabsons, M. D. Brand, A mitochondrial uncoupling artifact can be caused by expression of uncoupling protein 1 in yeast. *Biochem J* **356**, 779–789 (2001).

41. J. A. Stuart, J. A. Harper, K. M. Brindle, M. B. Jekabsons, M. D. Brand, Physiological levels of mammalian uncoupling protein 2 do not uncouple yeast mitochondria. *J Biol Chem* **276**, 18633–18639 (2001).

42. M. Way, B. Pope, J. Gooch, M. Hawkins, A. G. Weeds, Identification of a region in segment 1 of gelsolin critical for actin binding. *EMBO J* **9**, 4103–4109 (1990).

43. K. S. Echtay, Q. Liu, T. Caskey, E. Winkler, K. Frischmuth, M. Bienengräber, M. Klingenberg, Regulation of UCP3 by nucleotides is different from regulation of UCP1. *FEBS Lett* **450**, 8–12 (1999).

Acknowledgements

Competing interests: The authors declare no competing financial interests. **Data and materials availability**: All data are available in the main article or the supplementary information, and from the corresponding author upon reasonable request. Source data are provided with this paper. All RNA Seq data have been deposited into the gene expression omnibus (GEO) under the accession number GSE224318 (*Monodelphis domestica*) and GSE112582 (*Mus musculus*) **Additional information:** Supplementary information is available for this paper. Correspondence and requests for materials should be addressed to martin.jastroch@su.se.

Supplementary Materials:

Supplementary Figures S1-S7

Supplementary Tables S1-S4

References only cited in the SM: 34-43

Appendix file 1

Fig. 1. Development of sustained endothermy and UCP1 expression in the juvenile opossum (*M. domestica*). A. Juveniles are born immature and attach to the teats. B. Overview on age and tissue sampling. C. Body weights. D. Body length. E. Infrared imaging of eye temperatures shown after separation from the mother. F. Rectal body temperatures measured immediately post-mortem G. Detection of UCP1 mRNA with qPCR in multiple tissues. H. Longitudinal analysis of UCP1 mRNA in adipose tissue depots. ingAT – inguinal adipose tissue, isc AT – interscapular adipose tissue, asAT - anterior subcutaneous adipose tissue. Data are mean ± SEM.; n= 4-9. Statistical significance between groups is denoted by *p < 0.05, **p < 0.01, ****p < 0.0001. One-way ANOVA (Tukey's post-hoc test).

Fig. 2. Comparative analysis of the opossum adipose transcriptome reveals a rudimentary browning signature

A. To show commonly regulated genes in adipose tissue, the directed p-value of mouse BAT mRNAs (cold vs warm) was plotted against the p-value of opossum adipose mRNAs (6 vs 10 weeks old). Inter-species similarities are found in particular in the inguinal AT mRNAs. Significant overlap between Mouse and Monodelphis regulated genes passing FDR correction (squares), was estimated using a Hypergeometric distribution test. A significant overlap (p< 0.001) is indicated in red. B. Regulation of adrenergic receptors in opossum adipose tissue from 6 to 10 weeks of age. Box plots showing the distribution of log gene expression level. The central mark indicates the median, and the bottom and top edges of the box indicate the 25th and 75th percentiles, respectively. The whiskers extend to the most extreme data points. C. Heat map of cross-species and tissue comparisons of inguinal AT DEGs. D. Browning probability using the PROFAT tool. Data are mean ± SEM.; n= 4-5. B: Statistical significance between groups is

denoted by $*p < 0.05$, $**p < 0.01$, $****p < 0.0001$; Two-way Anova (Sidak). C was partially created with BioRender.com.

Fig. 3. Comparative respirometry demonstrates lack of thermogenic function of marsupial UCP1

A. Cartoon of reductionist approach expressing UCP1 variants in mammalian cell culture. B. Western blotting of 20 μg of protein lysate from low and high mouse UCP1-expressing HEK293 cells (MmUCP1; lanes 2-7) and various amounts of mouse UCP1 standard, using the anti-mouse UCP1 antibody. (C) Western blotting of 20 μg of protein lysate from opossum UCP1-expressing HEK293 cells (MdUCP1; lanes 2-4) and various amounts of opossum UCP1 standard, using the anti-opossum UCP1 antibody. D. Scheme of UCP1 regulation and time-lapse respiration measurement to obtain oxygen consumption rates (OCR). Arrows indicate the injections of oligomycin (OLIGO), UCP1 activator or vehicle control (NNA: nonanoic acid), dinitrophenol (DNP) and rotenone/antimycin A (ROT/AA). E - H. Aggregated respiration traces using nonanoic acid (NNA), palmitate or TTNPB as specific UCP1 activator. The red arrow indicates the injection of activator or vehicle in wells with empty vector control (EV ctrl), mouse (MmUCP1) low and high, as well as opossum (Md UCP1) expressing HEK293 cells. I. Bar chart of OCR upon activator or vehicle treatment. J. Measurement of mitochondrial membrane potential in isolated mitochondria using safranin O quenching. K. UCP1 structural model based on threading into the ANT model. Identical amino acids in white, similar in light blue, and dissimilar in dark blue. Data are shown as mean ± SEM.; E-I: n=7-15 well measured on three independent days; J: n=3 independent experiments. Statistical significance between groups is denoted by $**p < 0.01$, $****p < 0.0001$. I: Two-way ANOVA (Tukey's post-hoc test). A and D were partially created with BioRender.com.

Fig. 4. Construction and functional analysis of stem eutherian <mark>and therian</mark> ancestor UCP1

A. Phylogenetic tree of UCP1 depicting stem eutherian reconstruction. B. Oxygen consumption rates (OCR) of HEK293 cells expressing the empty vector control, mouse (Mm) UCP1 and <mark>reconstructed stem eutherian ancestor (Anc)</mark> UCP1. Red arrow indicates the injection of activator (TTNPB) or vehicle. C. Bar chart of OCR upon <mark>activator</mark> or vehicle treatment. <mark>D.</mark> Alignment summarizing differences of the stem eutherian ancestor UCP1 (Anc) to mouse UCP1 (Mm), opossum UCP1 (Md) and stem therian ancestor UCP1 (Th). <mark>E. Western blotting of 20 μg of protein lysate from transiently transfected HEK293 cells expressing opossum UCP1 (MdUCP1; lanes 2-3), stem therian ancestor UCP1 (ThUCP1; lane 4-5) and various amounts of opossum UCP1 standard (lane 6-8), using the anti-opossum UCP1 antibody. F. Oxygen consumption rates (OCR) of HEK293 cells expressing Md or</mark> ThUCP1. G. Key mitochondrial carrier structural features (PDB: 6GCI (*30*)). H. The cytoplasmic bonding network predicted in eutherian UCP1, differing from marsupial UCP1, reconstructed therian UCP1, and mammalian UCP2 and UCP3, which are all identical. Data are shown as mean ± SEM. <mark>B and C: n=3-5 per group; F: 8-12 per group.</mark> Statistical significance between groups is denoted by **p < 0.01, ****p < 0.0001. C: Two-way ANOVA (Tukey's post-hoc test).

Figure 1
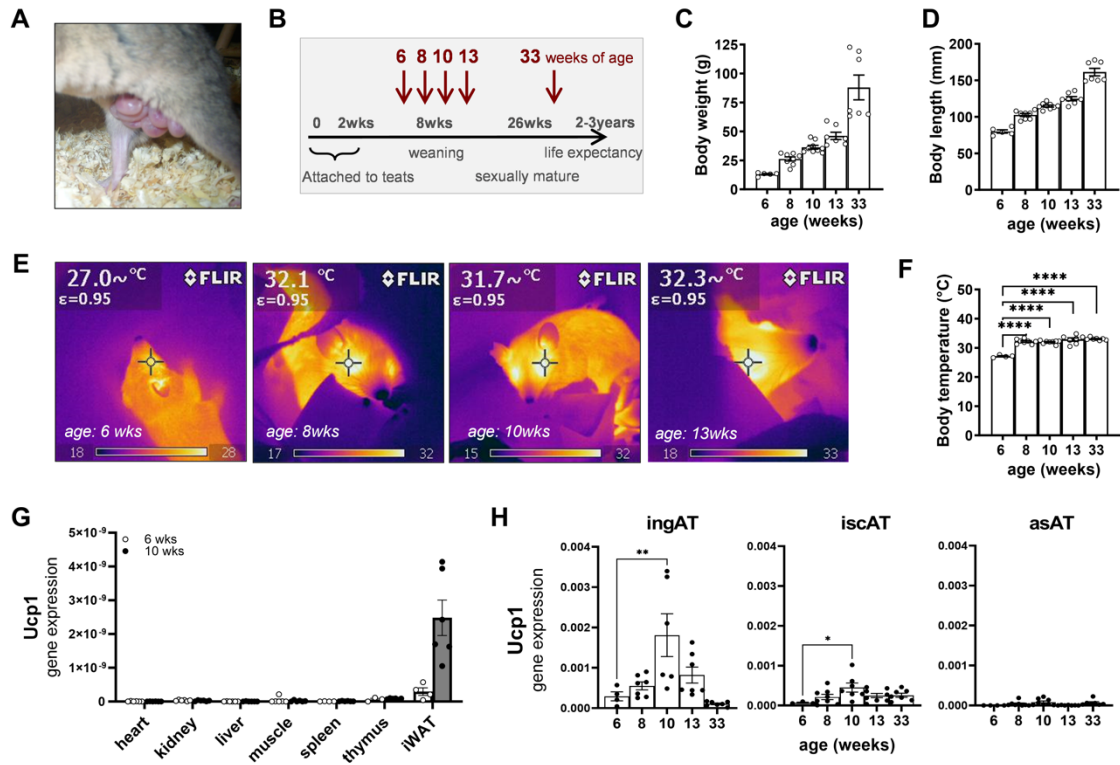
Figure 2
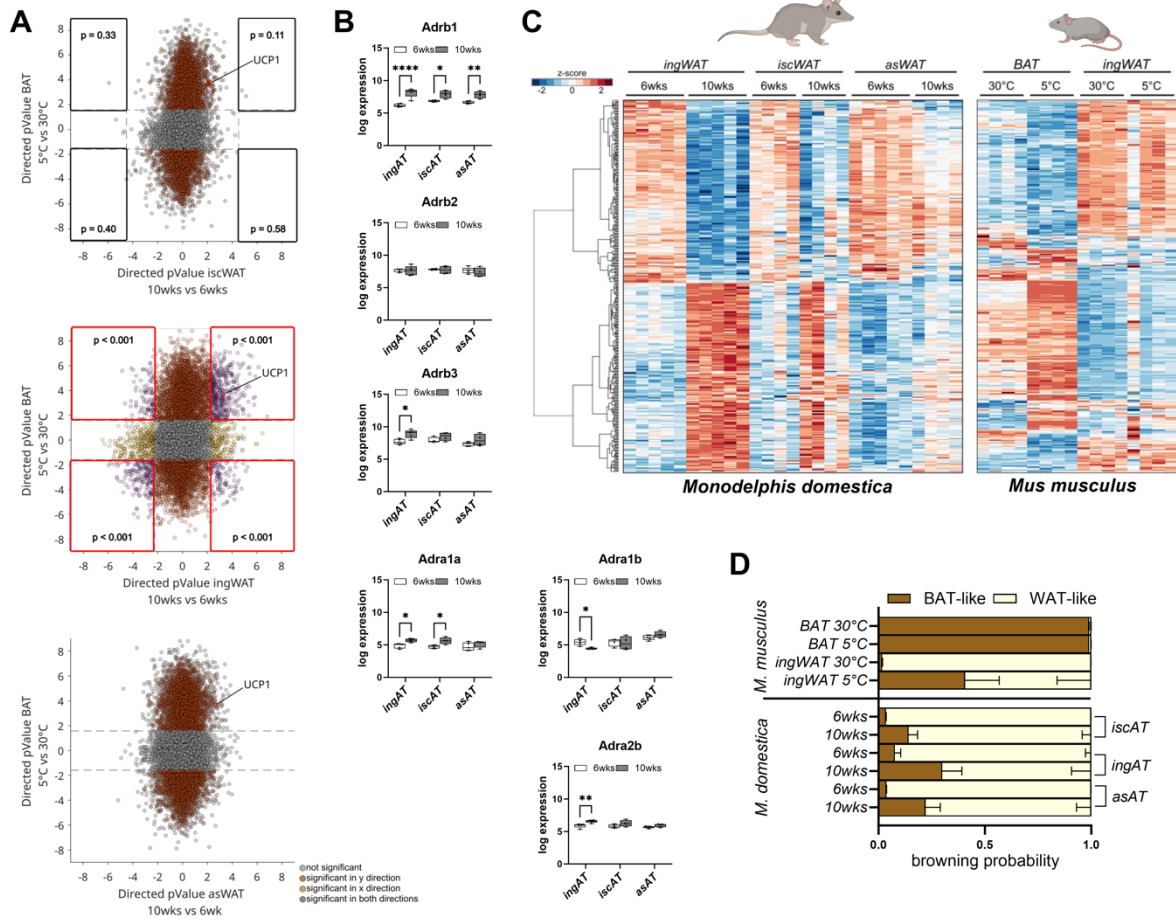
Figure 3

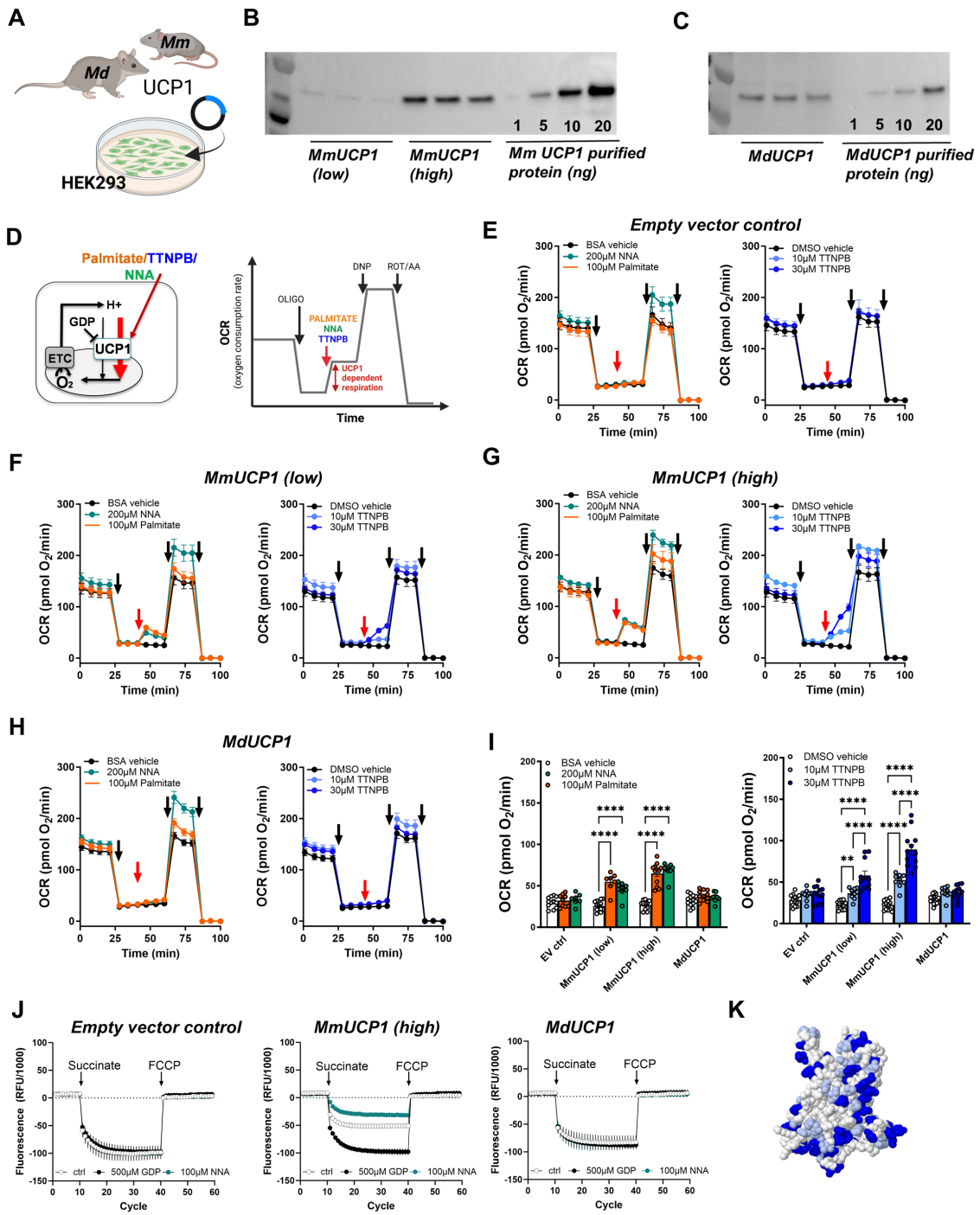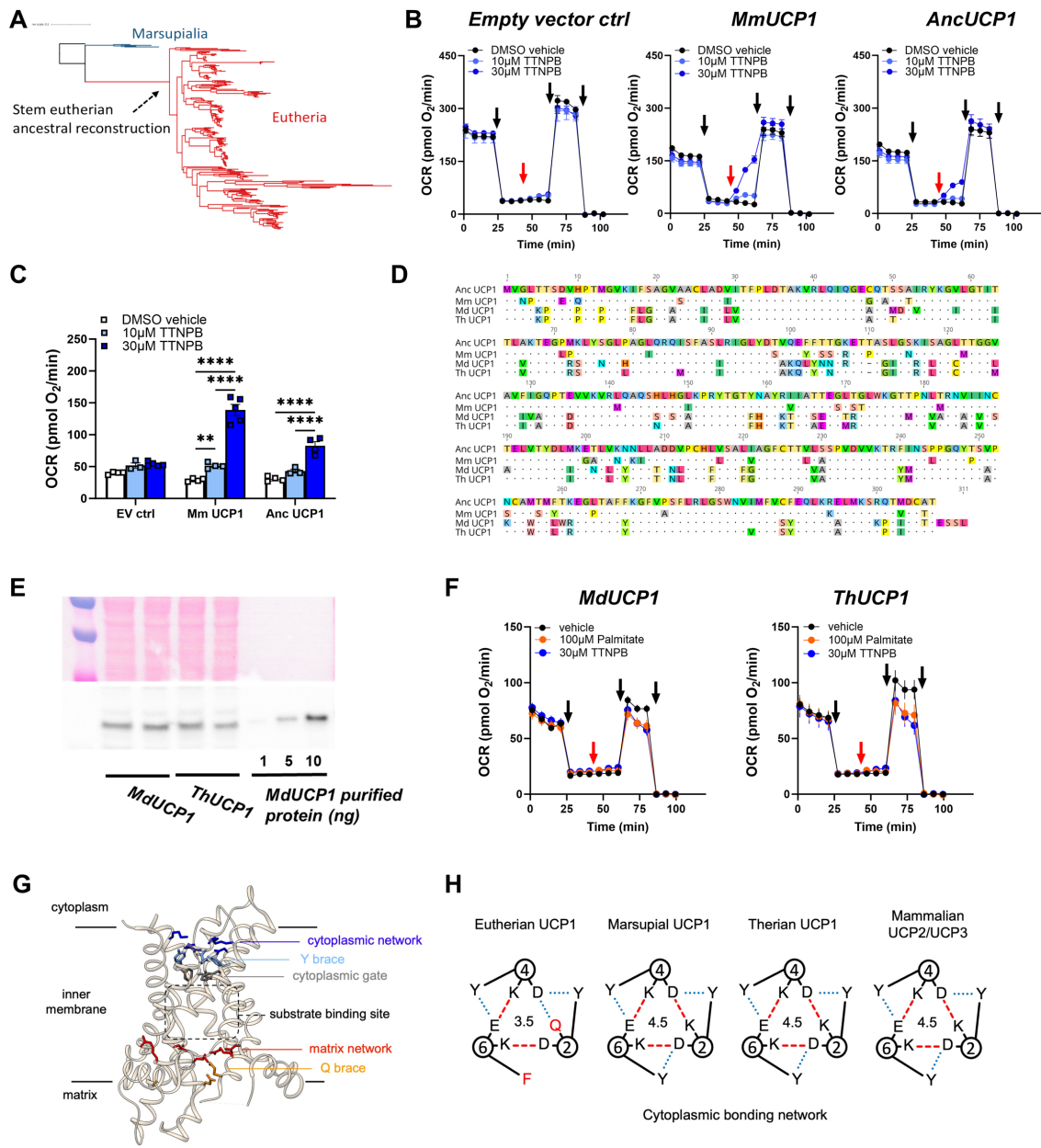# Figure 4

Supplementary Materials for

Two stage evolution of mammalian adipose tissue thermogenesis

Authors: Susanne Keipert†, Michael J. Gaudry†, Maria Kutschke, Michaela Keuper, Margeoux A.S. Dela Rosa, Yiming Cheng, José M. Monroy Kuhn, Rutger Laterveer, Camila A. Cotrim, Peter Giere, Fabiana Perocchi, Regina Feederle, Paul G. Crichton, Dominik Lutter, Martin Jastroch*

†contributed equally
*Corresponding author: martin.jastroch@su.se

The PDF file includes:

Materials and Methods

Study animals and maintenance

Experiments were performed on laboratory bred gray short-tailed opossum (*Monodelphis domestica*). The animals were obtained from the colony maintained at the Museum für Naturkunde (Museum of Natural History) in Berlin, and kept in type 4 cages with enrichment, at an ambient temperature of 26°C on a reverse 12:12 hrs light:dark cycle with ad libitum access to food and water. In this study we used differently aged animals (6, 8, 10, 13, and 33 week old males and females mixed in each group, n=4-9). We took infrared pictures (ThermaCAM, FLIR) pointed at the eyes and measured rectal body temperature immediately post mortem. Animals were killed with an overdose of isoflurane; body mass and length were measured, and blood and tissue samples collected for further analyses. The animal welfare authorities approved animal maintenance (ZH104), the procedures were executed under T0198/13.

Blood parameters

Commercially available kits were used for the analysis of serum NEFA (NEFA-HR2 Wako), and Triglycerides (LabAssay Triglyceride, GPO-DAOS method, Wako according to the manufacturer's recommendations).

Gene expression

RNA was extracted using Qiazol according to the manufacturer's instructions (Qiazol Lysis Reagent, Qiagen). Synthesis of cDNA and DNAse treatment was performed from 1 µg of total RNA using the QuantiTect Reverse Transcription Kit (Qiagen). The oligonucleotide primer sequences for real time qPCR, performed with SYBRgreen (Applied Biosystems or Biorad), can be found in Supplemental table 1 (Table S1).

Transcriptomic Analysis

RNA quantification and qualification (performed with commercial provider Novogene): RNA integrity was assessed using the RNA Nano 6000 Assay Kit of the Bioanalyzer 2100 system (Agilent Technologies, CA, USA). Library preparation for Transcriptome sequencing Total RNA was used as input material for the RNA sample preparations. Briefly, mRNA was purified from total RNA using poly-T oligo-attached magnetic beads. Fragmentation was carried out using divalent cations under elevated temperature in First Strand Synthesis Reaction Buffer (5X). First strand cDNA was synthesized using random hexamer primer and M-MuLV Reverse Transcriptase (RNase H-). Second strand cDNA synthesis was subsequently performed using DNA Polymerase

I and RNase H. Remaining overhangs were converted into blunt ends via exonuclease/polymerase activities. After adenylation of 3' ends of DNA fragments, Adaptor with hairpin loop structure were ligated to prepare for hybridization. In order to select cDNA fragments of preferentially 370~420 bp in length, the library fragments were purified with AMPure XP system (Beckman Coulter, Beverly, USA). Then, PCR was performed with Phusion High-Fidelity DNA polymerase, Universal PCR primers and Index (X) Primer. Finally, PCR products were purified (AMPure XP system) and library quality was assessed on the Agilent Bioanalyzer 2100 system.

Opossum RNA dataset: Sequencing reads were aligned against the *Monodelphis domestica* reference genome (ASM229v1) with STAR Mapper v2.7.8a (*34*) using Ensembl gene annotations. Count files were created using STAR counts. The *rlog* function of the R package DESeq2 (*35*) was used for variance stabilization of raw counts. Potential batch effects between the samples from both sequencing batches were removed using the *removedBatchEffect* function of the R package limma (*36*). Genes were filtered for low expression by removing all genes with a log expression below 2.5 in all samples. Additionally, MATLAB bioinformatics toolbox function *geneentropyfilter* was used to remove genes with entropy in the lowest 10 percent.

Mouse dataset: Count files for Mouse gene expression data were derived from Gene Expression Omnibus (GSE112582). Genes were filtered for low expression removing genes with a cumulative count sum < 100 and more that 5 samples with 0 counts. The *rlog* function R package DESeq2 (*35*) was used for variance stabilization of raw counts.

Ortholog gene mappings between *M. domestica* and *M. musculus* were obtained via the online tool OrthoVenn2 (*37*). Differential gene expression for *M. domestica* and *M. musculus* data was estimated using One-way ANOVA independent for each adipose tissue. Directed p-values were calculated as the –log10 of one-way ANOVA p-values multiplied by the sign of the log-foldchange. Heatmaps and dendrograms were calculated using MATLAB's *clustergram* function using ward linkage method.

To assess whether the overlap or enrichment of significantly regulated genes (squares), passing FDR correction, between Mouse and Monodelphis was higher than expected, we conducted a Hypergeometric distribution test (& Fisher exact test). A significant overlap was considered at p< 0.001.

Reconstruction of the ancestral eutherian and therian UCP1 sequence

The UCP1 coding sequence data set (*26*) was expanded to include 237 mammalian species using genome mining techniques (accession numbers are listed in Table S2). Species with previously described UCP1 pseudogenes (*26*) were excluded as mutations accumulated throughout the course of neutral evolution would likely bias the results. Sequence analyses were performed using Geneious 9.1.8. UCP1 coding sequences (Table S2, Appendix file 1) were aligned using MUSCLE (*38*), a tree was expanded from (*41*) based on previously published phylogenetic relationships (see Table S3 for references; ; Appendix file 1 for tree), and the ancestral sequence reconstruction was performed using PAML 4.8 (*39*) (Fig. S4, Appendix file 1). The reconstructed sequences were trimmed of insertions to match consensus UCP1 lengths and was artificially synthesized (Bio Basic) and cloned into the pcDNA3.1 vector as performed for MmUCP1 and MdUCP1 coding sequences. Stably expressing ancestral UCP1 HEK293 cell lines were generated as described and overexpression confirmed with primers in Table S1 (Fig. S5).

Stable expression of UCP1 orthologues in mammalian HEK293 cells

For analysis of UCP1 in HEK293 cells, the *Mus musculus* (MmUCP1), *Monodelphis domestica* UCP1 (MdUCP1) coding sequence (GenBank Accession number OP589293) and the reconstructed stem eutherian ancestor (AncUCP1) were cloned into a pcDNA3.1+ vector (containing geneticin-resistant gene), amplified in DH5a competent *E.coli* (Invitrogen), transfected into human embryo kidney cells (HEK293) and selected for stable expression (see (*15, 23*)). HEK293 cells were grown up to a confluency of 60-70% on 6-well plates and transfected with 2 μg of plasmid or an empty vector control (Viafect Transfection Reagent, Promega or PolyFect Transfection Reagent, Qiagen). After 24 hours cells were washed and new medium was added. On the third day after transfection, the cells were split, seeded on new 10 cm plates at a confluency of 20-30% and the selection process was started by adding 500 μg/ml geneticin to the medium. Positive clones were picked, cultured separately and the UCP1 expression was validated by immunological detection. The clones with a low and moderate expression of mouse UCP1 as well as moderate expression of Monodelphis UCP1 were used for further analysis. During geneticin-enrichment of UCP1-positive cells, vials were stored for the functional analysis of opossum UCP1-enriched cells.

Transient transfections of opossum and reconstructed stem therian ancestor UCP1

For the comparative assessment of opossum (Md UCP1) and reconstructed stem therian ancestor UCP1 (Th UCP1), HEK293 cells were cultured in T175 flasks in DMEM (4.5 g/L glucose, +L-

4

Glutamine, -Pyruvate, pH7.4 at RT [Gibco]) supplemented with 10% FBS (Gibco) and 1% penicillin/streptomycin (Gibco) at 37°C and 5% CO2. On the day of the transient transfections, the cells were trypsinized from the flasks with 0.05% trypsin-EDTA (Gibco) and counted in duplicate. The cells (2.46×10^6 total) were then aliquoted into 15 ml tubes in 4.48 ml of growth medium. Transfection mixtures were then prepared with 1260 µl DMEM, 12.6 µg plasmid DNA, and 50.4 µl Polyfect reagent (Qiagen) and incubated for 15 minutes at room temperature. Transfection mixtures were then added to the HEK293 cells in suspension and seeded on polyethyleneimine coated XFe96 plates at a density of 30000 cells/well or wells of a 12-well plate for RNA and protein isolation at a density of 430 cells/well. Plate-based respirometry experiments were performed 24 hours after transfection.

Plate-based respirometry

HEK293 cells were seeded on XF96 well culture plates (Agilent), which have been previously coated with polyethyleneimine (PEI; 1:15,000 dilution). DMEM (4.5 g/L glucose, +L-Glutamine, -Pyruvate, pH 7.4 at RT) supplemented with 10% FBS (Gibco) and 50 µg/mL geneticin (MmUCP1 HEK293, MdUCP1 HEK293, empty vector HEK293) was used for cell culturing. On the day of the assay (24 hours after seeding), cells were washed twice with assay medium (XF base Medium (Agilent), 10 mM glucose, 10 mM pyruvate, 2mM Glutamine, 0.4% BSA (w/v)) and then incubated in 180 µl of assay medium in an air incubator without CO_2 at 37°C for 1 hour. The XF96 plate was then transferred to a temperature-controlled (37 °C) XF96 or XFe96 Extracellular Flux Analyzer (Agilent). Four assay cycles (1-min mix, 2-min wait and 3-min measuring period) were used to determine basal respiration, and then oligomycin (4 µg/ml; inhibiting ATP synthase) was added by automatic pneumatic injection (three assay cycles). Next, different concentrations of TTNPB (4- 2-(5,6,7,8-tetrahydro-5,5,8,8-tetramethyl-2-naphthalenyl)-1-propenyl]benzoic acid) (10 and 30 µM diluted in dimethylsulphoxide), palmitate (100 µM; conjugated to 0.17 mM BSA) or nonanoic acid (100 and/or 200 µM) were injected, followed by an injection of DNP (dinitrophenol; 100 µM) to completely uncouple mitochondria. Each experimental trace was ended by final injection of a cocktail of rotenone (4 µM) and antimycin A (2 µM) to correct for non-mitochondrial respiratory rate.

Mitochondrial membrane potential

HEK293 cells were grown to confluency on PEI-coated plates. Cells were harvested and mitochondria were isolated according to (*23*). Mitochondrial protein concentration was determined

using the biuret method. Measurement of mitochondrial membrane potential was performed in a 96-well plate format at 37°C. 40 µg of mitochondria in KHE buffer (120 mM KCl, 5 mM KH2PO4, 3 mM HEPES, 1 mM EGTA, 0.4% BSA; pH 7.2), containing 1 µg/mL oligomycin, 4 µM rotenone, 100 nM nigericin and 5 µM safranin O, were added to each well. To determine the membrane potential after activation or inhibition of UCP1, 100 µM nonanoic acid or 500 µM guanosine diphosphate (GDP) were added, respectively. Fluorescence was detected in a CLARIOstar plate reader (BMG Labtech) using a 533-15 excitation and 576-20 emission filter. The cycle time was set to 20-21 seconds. After measuring basal fluorescence, 10 mM succinate was added to energize the mitochondria. Finally, the mitochondrial membrane was depolarized by the addition of 8 µM FCCP (carbonyl cyanide-p-trifluoromethoxyphenylhydrazone). Measurements were performed in duplicates on three independent days.

Establishment of monoclonal anti-UCP1 antibodies

A peptide (UCPB) comprising aa 236-252 (KTRYMNSPPGQYTSAPK) of UCP1 from *Monodelphis domestica* was synthesized and coupled to ovalbumin (Peps4LS, Heidelberg). Lou/c rats were immunized i.p. and s.c. with a mixture of 40µg peptide, 6nmol CpG (Tib Molbiol, Berlin) and inclomplete Freund's adjuvant. A boost without adjuvant was given 6 weeks after the primary injection and spleen cells were fused with myeloma cell line P3 × 63-Ag8.653 (ATCC, American Type Culture Collection) by standard procedures. Hybridoma supernatants were screened 10 day later in an ELISA assay for specific binding to biotinylated UCPB peptide on avidin-coated ELISA plates. Supernatants that specifically reacted with the UCPB peptide were further validated in Western blot analysis. Selected hybridoma cells were subcloned by at least two rounds of limiting dilution to obtain stable monoclonal cell lines. Experiments in this work were performed with hybridoma supernatant of clone UCPB 19E7 (rat IgG2c).

Recombinant UCP1 standards

UCP1 protein standards for the immunoblot quantification of expressed isoforms were generated in *E. coli* as described previously (*15, 40, 41*). Protein coding sequences for Mm UCP1 (mouse), Md UCP1 (opossum) and Anc UCP1 (stem eutherian ancestral reconstruction) were cloned into a pMW172 expression vector (*40–42*) with a < 10 amino acid N-terminal hexa-histidine-tag included at the 5'-end using standard molecular biology methods. Each isoform was expressed in *E. coli* (strain C41 (DE3)) and inclusion bodies were isolated using established methods (*43*). The his-tagged proteins were purified by Ni-NTA affinity chromatography under denaturing conditions as

recommended by the manufacturer (Qiagen). Inclusion bodies were resuspended in 10 ml lysis buffer (100 mM Tris HCl (pH 8.0), 8 M urea, 100 mM NaH2PO4) and centrifuged at 15,500 x g, 10 minutes at 4C. The clarified supernatant was sterile-filtered to remove particulates prior to application onto 1 ml Ni-NTA Superflow cartridge (Qiagen) (pre-equilibrated with lysis buffer). Clarified supernatant was passed through the column, at a flow rate of 1 ml/minute using a peristaltic pump. Contaminants were removed with 10 ml wash buffer (100 mM Tris HCl (pH 6.3), 8 M urea, 100 mM NaH2PO4) and histidine-tagged UCP1 protein was eluted from the column with 10 ml elution buffer (100 mM Tris HCl (pH 4.5), 8 M urea, 100 mM NaH2PO4). Eluates were concentrated to ~1 ml by centrifugal filtration (Vivaspin concentrators, MWCO 30,000 Da) and diluted with 9 ml resuspension buffer 1 (20 mM Tris HCl (pH 8.0), 2% (w/v) sarkosyl), to remove bulk urea, before being concentrated to ~1 ml again. The eluates were then diluted with 9 ml resuspension buffer 2 (20 mM Tris HCl (pH 8.0), 0.5% (w/v) sarkosyl) and concentrated to ~1 ml again. The resulting eluates were applied onto a PD10 column (pre-equilibrated with resuspension buffer 2) to remove residual urea. The final protein concentration of purified samples was quantified by BCA assay. The purified protein standards were snap-frozen and stored at -80C until further use.

Western blot

Protein lysates were prepared from frozen cells using RIPA Buffer (150mM NaCl, 1% IGEPAL CA-630, 0,5% sodium deoxycholate, 0,1% SDS, 50mM Tris, pH 8.0) containing 1x protease-/phosphatase inhibitors. All steps were performed on ice or at 4 °C. Protein concentration of the samples was quantified using the Bradford method (B6916, Sigma). For the analysis of UCP1 protein expression, 20µg total protein were electrophoresed in a SDS-polyacrylamide gel (4-12% Bis-Tris, Invitrogen by Thermo Fisher Scientific) and blotted on a nitrocellulose membrane (iBlot 2NC Regular Stacks, Invitrogen by Thermo Fisher Scientific). Immunoblots were performed using following antibodies; anti- UCP1 (R&D Systems, MAB6158, RRID:AB_10572490 R&D Systems), anti-UCP1 (Abcam, ab 155117, AbcamRRID:AB_2783809) and anti- UCPB 19E7.

Statistics

Statistical analyses were performed using Stat Graph Prism 9 or 10 (GraphPad Software, San Diego, CA USA). 1-way or 2-way ANOVA and Tukey's, or Sidak's or Dunetts multiple comparisons test were used to determine differences between the groups. Statistical significance

was assumed at $p < 0.05$. Statistical significance is denoted by *$p < 0.05$, **$p < 0.01$, ***$p < 0.001$, ****$p < 0.0001$.

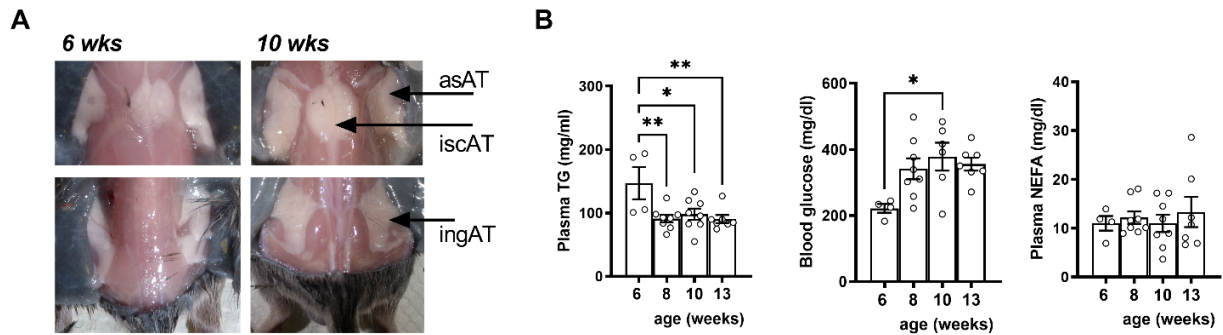Supplemental Figures

Figure S1:

Figure S1 (related to Figure 1): (A) Representative pictures of different adipose tissue depots of a 6wks vs 10 wks old opossums (*M. domestica*) (as – anterior subcutaneous, isc- interscapular, ing – inguinal, AT – adipose tissue). (B) Plasma Triglycerides (TG), blood glucose and plasma non-esterified fatty acids (NEFA) of different aged opossums. Data are mean ± SEM.; n= 4-8. One-way ANOVA (Tukey's post-hoc test). Statistical significance between groups are denoted by *$p < 0.05$, **$p < 0.01$.
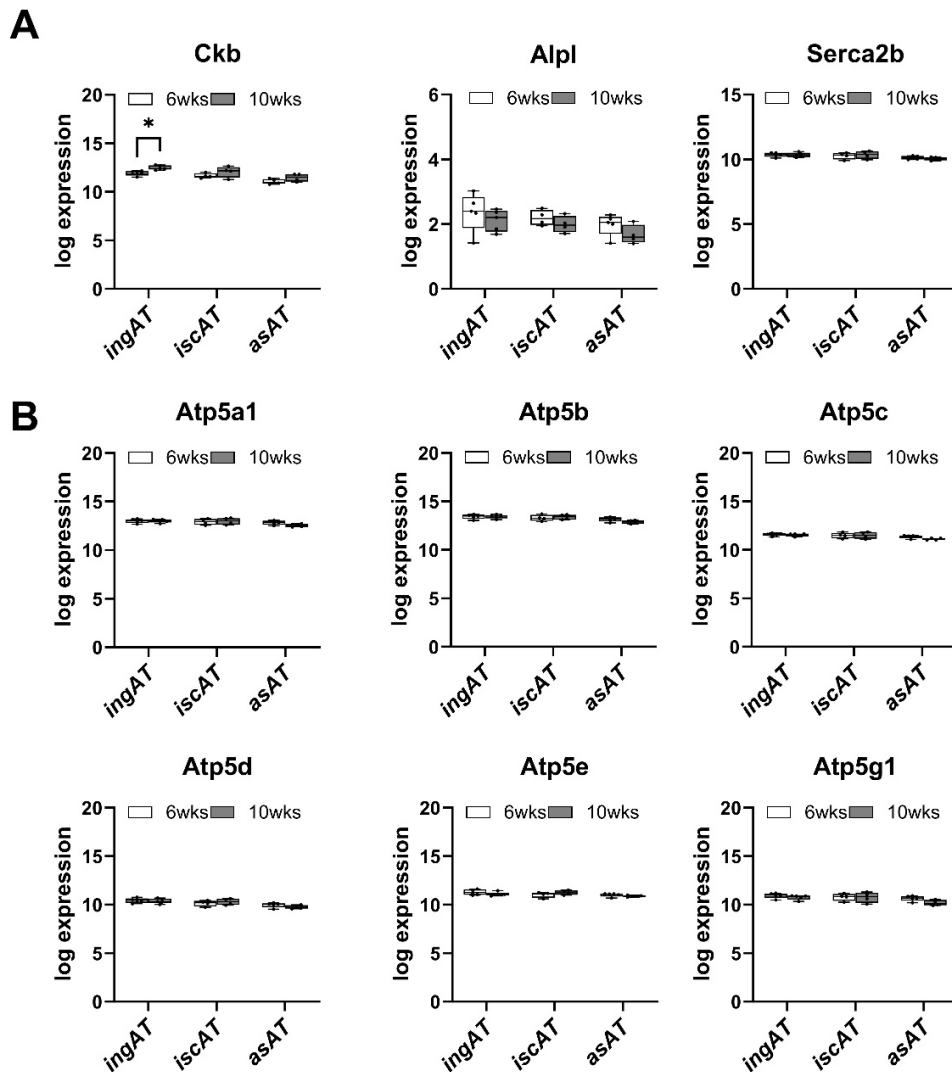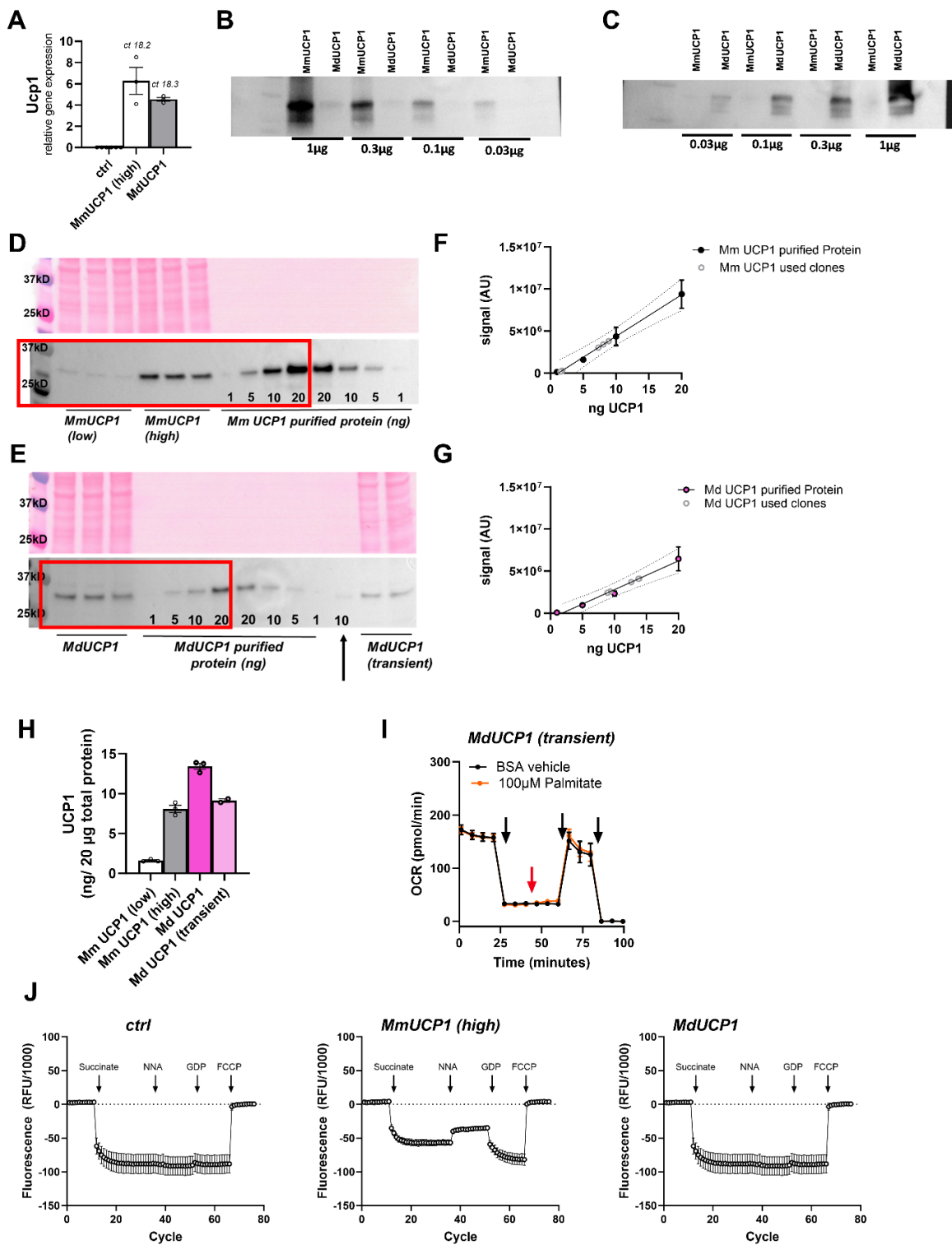
A

B

Figure S3 (related to Figure 3): (A) UCP1 mRNA expression of empty vector (ctrl), mouse UCP1 (MmUCP1) and opossum UCP1 (MdUCP1) in HEK293 cells assessed with qPCR (n=3 per group). (B) Western blot of different amounts of mouse or opossum UCP1 standard, probed with the anti-mouse UCP1 antibody (Abcam, ab 155117) (C) Western blot of different amounts of mouse and opossum UCP1 standard, probed with the opossum UCP1-specific antibody (UCPB 19E7). (D) Western blotting of 20 µg of protein lysate from low and high mouse UCP1-expressing HEK293 cells (lanes 2-7) and various amounts of mouse UCP1 standard, using the anti-mouse UCP1 antibody. (E) Western blotting of 20 µg of protein lysate from opossum UCP1-expressing HEK293 cells (lanes 2-4) and various amounts of opossum UCP1 standard, using the anti-opossum UCP1 antibody (n=3 per group). Red frames in (D) and (E) depict the cropped section used for main Figure 3. (F) Densitometric analysis of mouse UCP1 concentrations using the mouse UCP1 standard. (G) Densitometric analysis of opossum UCP1 concentrations using the opossum UCP1 standard. (H) Bar chart depicting UCP1 concentrations of the HEK293 cells. (I) Plate-respirometry of transiently transfected opossum HEK293 cells, partially enriched by high antibiotic selection pressure. Averaged OCR traces upon vehicle (BSA control) or 100 µM palmitate injection (indicated by the red arrow) (n = 7-9 per group). (J) Measurement of mitochondrial membrane potential (using safranin O) of isolated mitochondria from empty vector control (ctrl), high mouse UCP1 (Mm) and opossum UCP1 (Md)-expressing cells. Injections where indicated of nonanoic acid (NNA), guanosine diphosphate (GDP), and FCCP (n=3 per group). Data are mean ± SEM.
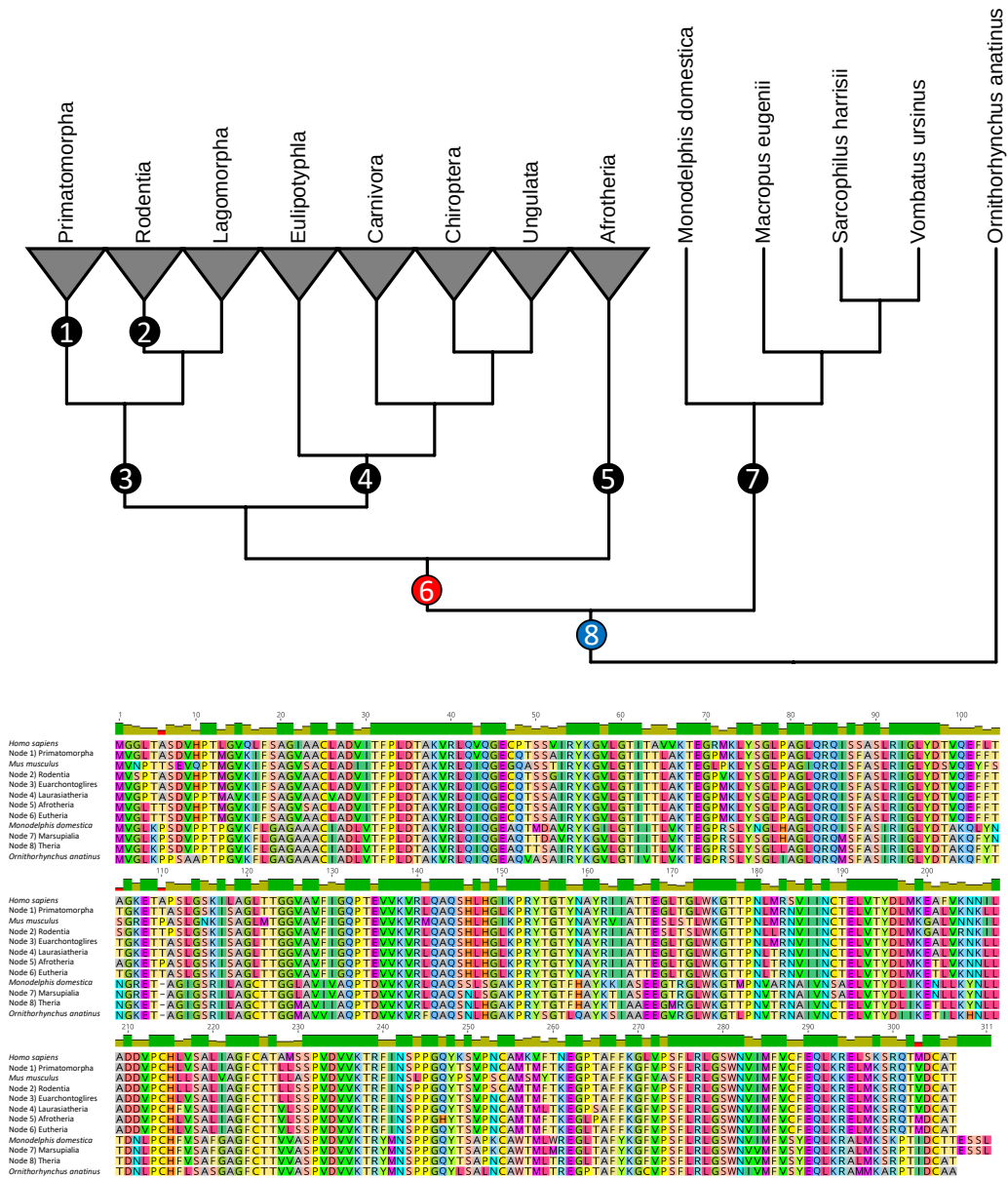
Figure S4 (related to Figure 4): Ancestral sequence reconstruction of mammalian UCP1 performed using phylogenetic analysis by maximum likelihood (PAML). Reconstructed UCP1 from major nodes of the mammalian phylogenetic tree are aligned against modern UCP1 variants of the human (*Homo sapiens*), mouse (*Mus musculus*), opossum (*Monodelphis domestica*), and platypus (*Ornithorhynchus anatinus*). Node 6, indicated in red, is that of the stem eutherian ancestor and node 8, indicated in blue, is that of the stem therian ancestor.

Figure S<mark>5</mark>:
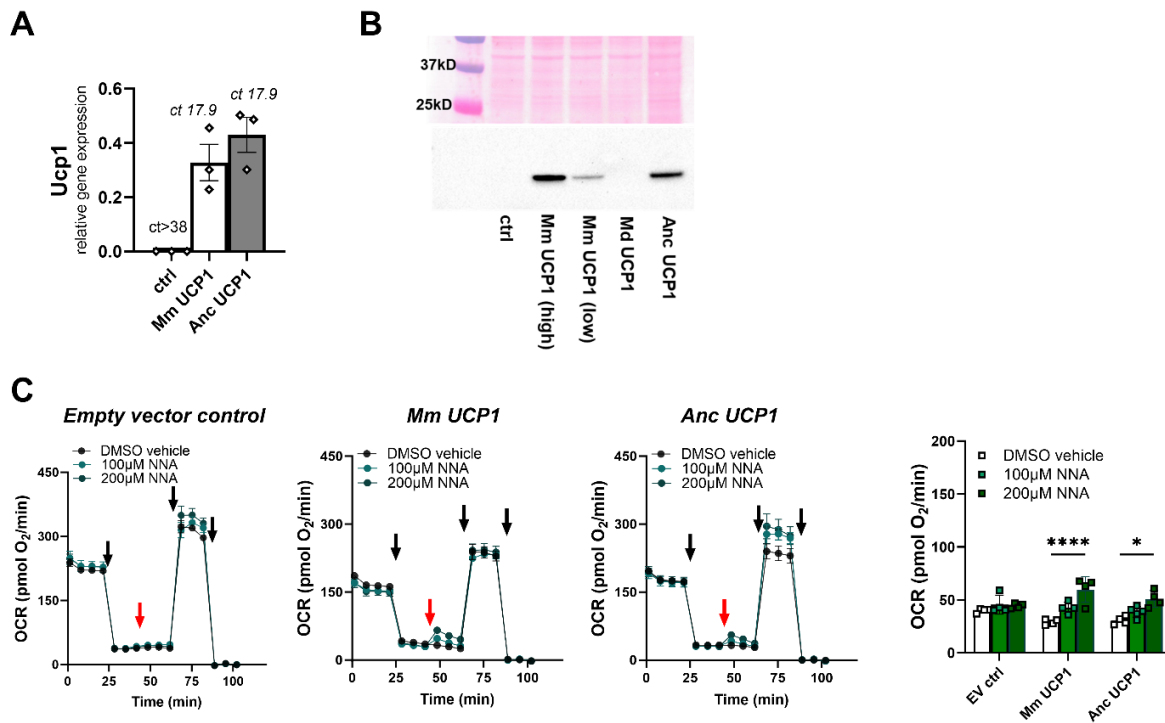
Figure S5 (related to Figure 4): (A) UCP1 mRNA expression of empty vector (ctrl), mouse UCP1 (MmUCP1) or stem eutherian ancestral reconstruction UCP1 (Anc UCP1) in HEK293 cells assessed with qPCR (n=3 per group). (B) Western blot detection of UCP1 in HEK293 expressing empty vector (ctrl), mouse UCP (Mm UCP1 low and high expresser), opossum UCP1 (Md UCP1) and stem eutherian ancestral reconstruction UCP1 (Anc UCP1), using an anti-mouse UCP1 antibody (R&D Systems, MAB6158, RRID:AB_10572490 R&D Systems). (C) Plate-based respirometry of HEK293 clones transfected with empty vector (ctrl), mouse UCP1 (Mm; high expresser) and stem eutherian ancestral reconstruction UCP1 (Anc). Averaged OCR traces upon vehicle or nonanoic acids (NNA) injection (n = 3-5 per group). Data are presented as means ± s.e.m. Statistical significance between groups are denoted by *p < 0.05, ****p < 0.0001. Two-way ANOVA (Tukey's post-hoc test).

Figure S6:
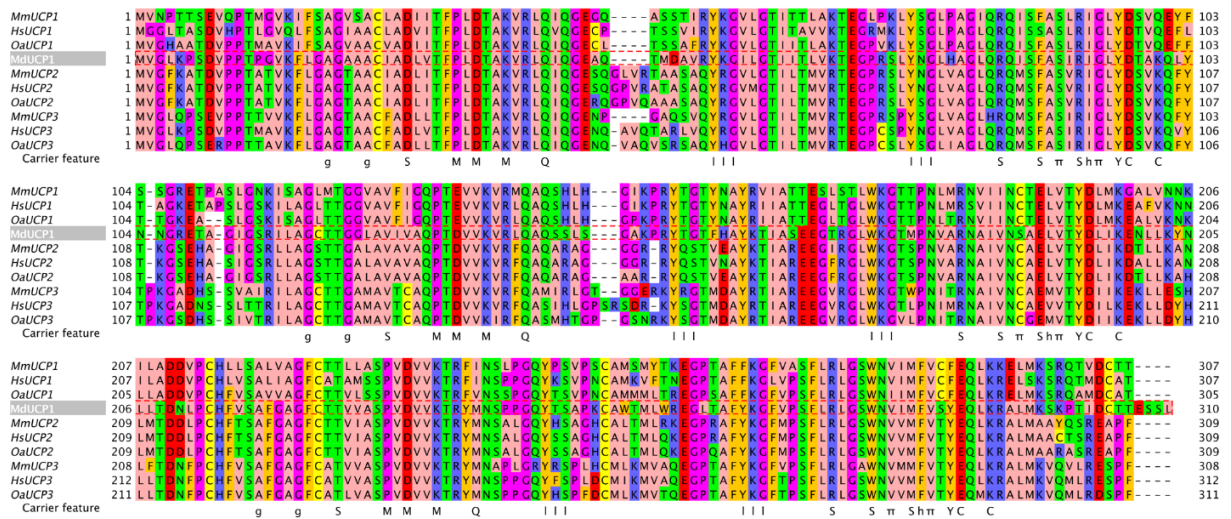
Figure S6 (related to Figure 4): The conservation of structural elements between MdUCP1 and selected eutherian UCP1, 2 and 3 proteins indicated by amino acid sequence alignment. UCP1 from *Monodelphis domestica* (Md; grey highlight/dashed box) was aligned with UCP1, 2 and 3 sequences from *Mus musculus* (*Mm*) *Homo sapiens* (*Hs*) *Ovis aries* (*Oa*) using the Muscle alignment algorithm. Amino acids are coloured according to their physicochemical properties. The position of residues corresponding to those involved in key mitochondrial carrier structural features (see (*14*) for details) are indicated: matrix salt bridge network formation (M) and supporting glutamine brace (Q); cytoplasmic salt bridge network formation (C) and supporting tyrosine brace (Y); carrier substrate binding region and central cavity-oriented residues (S); cardiolipin binding motifs (l); GxxxG (g) and πxxxπ (π) intra-domain interface motifs; cytoplasmic gate/hydrophobic plug (h).

Figure S7:

YD **K**

Identity

Monotremes
- Platypus
- Short-beaked echidna

Marsupials
- American
  - Gray short-tailed opossum
  - Monito del monte
- Australian
  - Tasmanian wolf
  - Yellow-footed antechinus
  - Numbat
  - Eastern quoll
  - Tasmanian devil
  - Common wombat
  - Common brushtail possum
  - Western ringtail possum
  - Leadbeater's possum
  - Rufous hare-wallaby
  - Western grey kangaroo
  - Eastern grey kangaroo
  - Brush-tailed bettong

g   g   S   M M M Q   l l l   l l l   S   S π Shπ **YC C**

YD K

Identity

g   g   S   M M M Q   l l l   l l l   S   S π Shπ **YC C**

Y**E** K

Identity

g   g   S   M M M Q   l l l   l l l   S   S π Shπ **YC C**
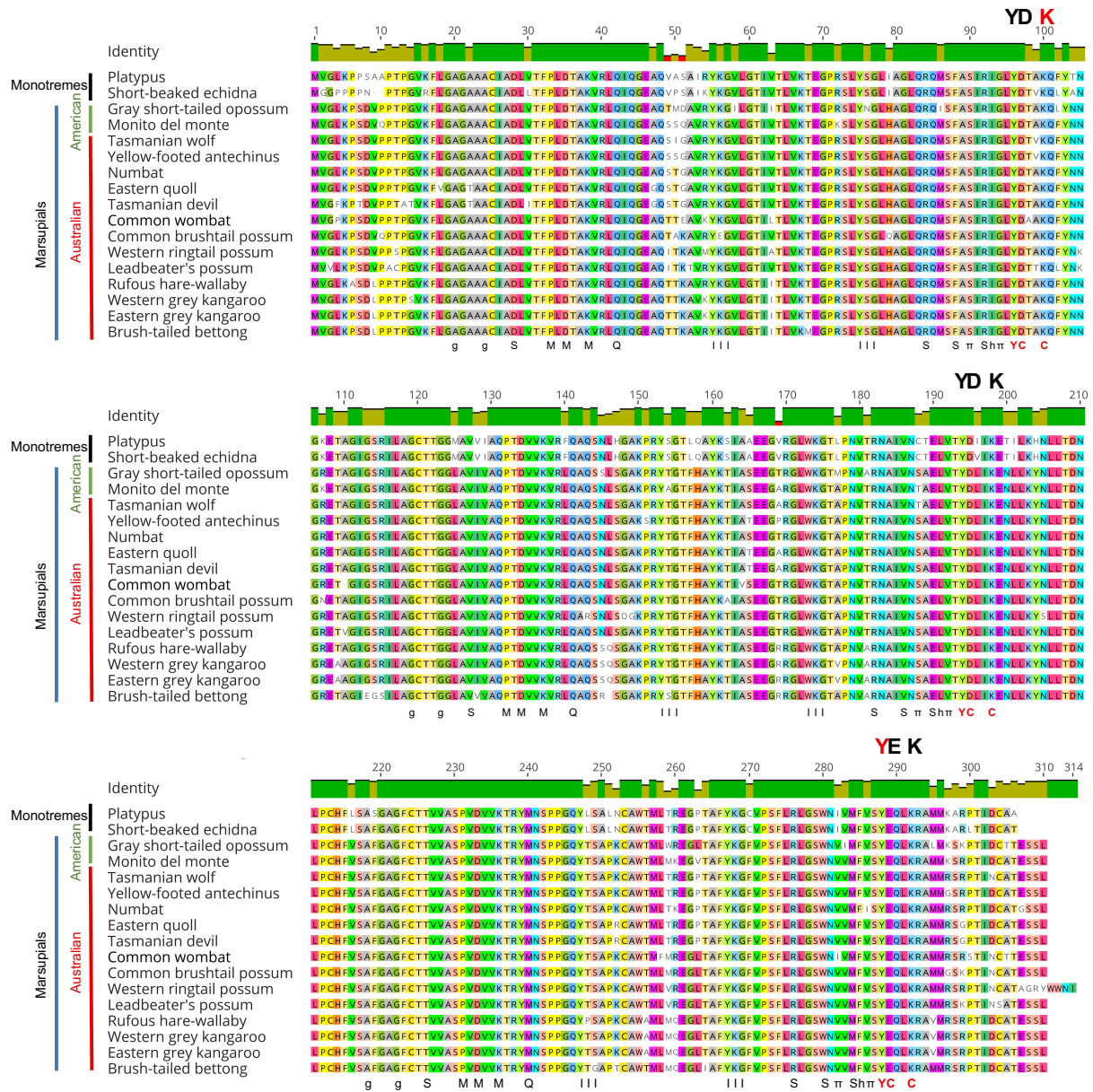
Figure S7 (related to Figure 4): The conservation of structural elements of UCP1 among monotremes (diverged prior to therians) and marsupials. Sequences were virtually translated from genomic contigs listed in Table S4. The residues involved in key mitochondrial carrier structural features (see (*14*) for details) are indicated: matrix salt bridge network formation (M) and supporting glutamine brace (Q); cytoplasmic salt bridge network formation (C) and supporting tyrosine brace (Y); carrier substrate binding region and central cavity-oriented residues (S); cardiolipin binding motifs (l); GxxxG (g) and πxxxπ (π) intra-domain interface motifs; cytoplasmic gate/hydrophobic plug (h). Residues of the cytoplasmic bridge network and supporting tyrosine

15

braces (highlighted above as YD/ExxK motifs) are conserved among monotremes and marsupials, but K100 and Y288 (highlighted in red) are mutated among eutherian mammals.

Supplemental Tables:

Table S1 Primers used for qPCR

Mm UCP1 F	5'-GGCCTCTACGACTCAGTCCA-3'
Mm UCP1 R	5'-TAAGCCGGCTGAGATCTTGT-3'
Anc UCP1 F	5'-AGAAGGGCCAATGAAACTCTAC-3'
Anc UCP1 R	5'-TTGTTAAGCCAGCTGAGATCT-3'
Md UCP1 F	5'-CTGCCAAACAGCTCTACAAC-3'
Md UCP1 R	5'-TGTGCTTGGAGTCTGACTTT-3'
Mm_Md UCP1 F	5'-TCTCCAGTGGATGTGGTAAA-3'
Mm_Md UCP1 R	5'-CACAAACATGATGACGTTCCA-3'
Md Cyclophilin A F	5'-GCCAACCCGAACGTGTACTT-3'
Md Cyclophilin A R	5'-GCCAACCCGAACGTGTACTT-3'
Human HPRT F	5'-CCTGGCGTCGTGATTAGTGAT-3'
Human HPRT R	5'-AGACGTTCAGTCCTGTCCATAA-3'
Human RSP13 F	5'-CTTGTGCAACACCATGTGAA-3'
Human RSP13 R	5'-CCCCACTTGGTTGAAGTTGA-3'

Table S2 Accession numbers of data-mined UCP1 containing contigs used for ancestral sequence reconstruction (see appendix 1 for alignment).

Ornithorhynchus anatinus	PTTO01001633.1
Vombatus ursinus	UNPS02014784.1, UNPS02005236.1
Sarcophilus harrisii	AFEY01396144.1, AFEY01173533.1, AFEY01430432.1
Macropus eugenii	ABQO020162103.1, ABQO020106554.1, ABQO020217652.1, ABQO020051005.1, ABQO021017422.1
Monodelphis domestica	AAFR03015618.1, AAFR03050488.1
Mus musculus	AEKQ02007025.1, AEKQ02091193.1, AEKQ02091194.1
Eulemur fulvus	PVJU010006755.1, PVJU010037679.1
Homo sapiens	ADDF02161735.1
Perognathus longimembris	RJWR010021414.1, RJWR010031543.1, RJWR010166025.1, RJWR010044175.1, RJWR010026110.1
Cebus capucinus	LVWQ01003314.1
Colobus angolensis	JYKR01122838.1, JYKR01122839.1, JYKR01122837.1
Marmota marmota	CZRN01000015.1
Macaca fuscata	BFBW01016187.1
Peromyscus polionotus	RCWS02238332.1, RCWS02238331.1, RCWS02108363.1, RCWS02108362.1
Peromyscus maniculatus	AYHN01134223.1, AYHN01134224.1, AYHN01057054.1
Nycticebus coucang	PVIV010023975.1, PVIV010029120.1, PVIV010013018.1, PVIV010001085.1
Gorilla gorilla	CYUI03000191.1
Macaca mulatta	AEHK01287844.1, AEHK01287845.1
Pan troglodytes	AACZ04031101.1
Galeopterus variegatus	JMZW01045216.1, JMZW01045217.1
Grammomys surdaster	SRMG01015776.1, SRMG01000098.1
Cuniculus paca	RJWT010005774.1
Tupaia tana	RJWV013127287.1, RJWV010409607.1, RJWV010370235.1, RJWV010155537.1
Dasyprocta punctata	RJWM01002178.1, RJWM01052513.1
Capromys pilorides	PVKN010122158.1, PVKN010431828.1
Allactaga bullata	PVKW010057424.1, PVKW010054471.1
Aplodontia rufa	PVKS010165543.1, PVKS010036019.1
Alouatta palliata	PVKV010011832.1
Cercopithecus neglectus	PVKI010035557.1, PVKI010063421.1
Cavia tschudii	PVKK010010314.1

Graphiurus murinus	PVLC010042589.1
Dinomys branickii	PVLD010006134.1
Cricetomys gambianus	PVKD010008737.1, PVKD010002359.1
Hydrochoerus hydrochaeris	PVLA01005061.1, PVLA01000658.1, PVLA01018335.1
Dolichotis patagonum	PVJX010005844.1, PVJX010035257.1, PVJX010016777.1
Ctenodactylus gundi	PVKB01003423.1
Muscardinus avellanarius	PVJB01027582.1, PVJB01002495.1
Petromus typicus	PVIR01011818.1
Hystrix cristata	PVJO010010249.1
Onychomys torridus	PVIT010277336.1, PVIT010047811.1
Pithecia pithecia	PVIP01016200.1, PVIP01016628.1
Saguinus imperator	PVHO010009192.1
Ateles geoffroyi	PVHS01003070.1
Zapus hudsonius	PVHP010000978.1
Xerus inauris	PVHX01003221.1, PVHX01022716.1, PVHX01020368.1
Dipodomys stephensi	PVHN010001068.1
Marmota flaviventris	QZWP01004518.1, QZWP01004517.1
Mus spicilegus	QGOO01037035.1, QGOO01037449.1
Piliocolobus tephrosceles	PDMG02000068.1
Ondatra zibethicus	PVIU01004088.1, PVIU01000508.1
Octomys mimax	NDGM010853922.1, NDGM010813548.1, NDGM011094622.1
Myocastor coypus	PVJA010005053.1
Sigmodon hispidus	PVIH01008922.1, PVIH01011225.1, PVIH01000848.1
Psammomys obesus	NESX01022721.1, NESX01013219.1
Mus pahari	FMBV02006289.1, FMBV02007694.1
Ellobius talpinus	LOJH01032235.1, LOJH01204927.1, LOJH01002093.1, LOJH01022825.1
Ellobius lutescens	LOEQ01000193.1, LOEQ01001200.1
Carlito syrichta	ABRT02355485.1, ABRT02355484.1
Microtus agrestis	LIQJ01004042.1, LIQJ01014426.1
Apodemus sylvaticus	LIPJ01184746.1, LIPJ01014497.1, LIPJ01000433.1, LIPJ01041350.1
Eulemur flavifrons	LGHW01000184.1
Eulemur macaco	LGHX01000184.1
Spermophilus dauricus	AXRT01069389.1, AXRT01456786.1, AXRT01126634.1, AXRT01490115.1

Mandrillus leucophaeus	JYKQ01107155.1, JYKQ01107156.1
Indri indri	RJWJ010111110.1 , RJWJ010099081.1 , RJWJ010088267.1, RJWJ010159983.1, RJWJ010054771.1
Mus caroli	FMAL02012098.1
Cavia aperea	AVPZ01000778.1
Lepus americanus	PVJM010078758.1, PVJM010050201.1, PVJM011081977.1, PVJM010074718.1, PVJM010056593.1, PVJM010022321.1, PVJM010244725.1, PVJM010025717.1, PVJM010610562.1, PVJM010610561.1, PVJM010405723.1
Mirza coquereli	PVHQ01011522.1
Propithecus coquereli	JZKE01017272.1, JZKE01017271.1, JZKE01274356.1, JZKE01017273.1
Meriones unguiculatus	PVJK01011688.1, PVJK01000020.1
Prolemur simus	MPIZ01119415.1, MPIZ01115442.1, MPIZ01109964.1, MPIZ01001557.1
Erythrocebus patas	PVJV010002478.1
Mandrillus sphinx	SRPC01051873.1
Cheirogaleus medius	PVHR01006358.1
Rhizomys pruinosus	PVIM010746246.1, PVIM010110035.1, PVIM011210680.1, PVIM010836851.1, PVIM010828812.1, PVIM013299969.1
Pygathrix nemaeus	PVHW010000773.1
Tympanoctomys barrerae	NDGN010056972.1, NDGN010566316.1, NDGN011149133.1, NDGN011128630.1, NDGN011472918.1, NDGN011276414.1
Fukomys damarensis	NP_000791.1
Neotoma lepida	LZPO01075894.1
Acomys cahirinus	PVKX01060493.1, PVKX01029987.1, PVKX01009175.1, PVKX01014858.1
Theropithecus gelada	QGDE01000005.1
Plecturocebus donacophilus	PVKP010017222.1, PVKP010044453.1, PVKP010044453.1
Marmota himalayana	RAQP01000038.1
Aotus nancymaae	JYKP02023189.1
Ctenomys sociabilis	PVKA01000751.1
Cercocebus atys	JZLG01060688.1
Macaca nemestrina	JZLF01028562.1
Phodopus sungorus	MCBN011415664.1, PVIM013299969.1, MCBN010997642.1,
Urocitellus parryii	QVIC01000044.1

Chlorocebus sabaeus	AQIB01017419.1
Tupaia chinensis	ALAR01031044.1
Myodes glareolus	MULK01009372.1, MULK01011956.1
Mus spretus	LVXV01001867.1, LVXV01010741.1
Nannospalax galili	AXCS01128924.1, AXCS01128925.1
Mesocricetus auratus	NM_001281332.1
Daubentonia madagascariensis	PVJZ01001121.1
Octodon degus	AJSA01193671.1, AJSA01193670.1, AJSA01174660.1
Microtus ochrogaster	AHZW01157106.1, AHZW01107615.1
Jaculus jaculus	AKZC01091543.1, AKZC01100636.1, AKZC01100630.1, AKZC01100628.1
Pan paniscus	AJFE02070950.1
Chinchilla lanigera	AGCD01027652.1, AGCD01027651.1
Rhinopithecus bieti	MCGX01002939.1
Castor canadensis	PVKL01000001.1
Semnopithecus entellus	PVII010000380.1
Rhinopithecus roxellana	JABR01098768.1
Nasalis larvatus	PVIX01003672.1
Cebus albifrons	PVKJ010004293.1
Thryonomys swinderianus	PVIC010028705.1
Glis glis	PVJS01008909.1
Heterocephalus glaber	AFSB01162372.1
Saimiri boliviensis boliviensis	AGCE01051213.1
Cricetulus griseus	FYBK01046174.1, FYBK01033961.1
Microcebus murinus	ABDC03018673.1
Macaca fascicularis	CAEC01514737.1
Dipodomys ordii	ABRO02057411.1
Ochotona princeps	ALIT01060999.1, ALIT01113862.1, ALIT01070725.1, ALIT01070720.1
Nomascus leucogenys	ADFV01177960.1, ADFV01177959.1
Ictidomys tridecemlineatus	AGTP01049379.1
Otolemur garnettii	AAQR03074138.1
Callithrix jacchus	XM_002745333.3
Papio anubis	AHZZ02027892.1
Lemur catta	PVHV01001186.1
Pongo abelii	NDHI03003363.1, NDHI03003437.1

Oryctolagus cuniculus	NM_001171077.1
Cavia porcellus	AAKN02011801.1
Rattus norvegicus	AAHX01097782.1, AAHX01007467.1, AAHX01007471.1
Canis lupus	QKWQ01000810.1, QKWQ01001430.1
Odocoileus hemionus	RCHL01005053.1
Rhinolophus ferrumequinum	AWHA01040305.1, AWHA01040304.1
Panthera tigris	ATCQ01112915.1
Cervus elaphus	MKHE01000005.1
Murina aurata	PVJC01048435.1
Solenodon paradoxus	RJWH01000799.1, RJWH01000121.1
Ursus arctos	QXTK01003749.1, QXTK01009164.1
Taxidea taxus	RCUC01068832.1
Ailurus fulgens	LNAC01000019.1
Ovis canadensis	PVIS010000157.1
Dicerorhinus sumatrensis	PEKH010008988.1
Bison bison	JPYT01100523.1, JPYT01019071.1, JPYT01642782.1
Enhydra lutris	NSES01008995.1
Odocoileus virginianus	MLBE01020605.1, MLBE01033370.1, MLBE01013100.1, MLBE01035654.1
Vicugna pacos	JEMW01007827.1
Ovis aries	CBYI010017988.1
Crocidura indochinensis	PVKC010006766.1, PVKC010126009.1, PVKC010074716.1, PVKC010349470.1, PVKC010175828.1
Craseonycteris thonglongyai	PVKE010001787.1
Hipposideros galeritus	PVLB01025537.1, PVLB01210632.1, PVLB01169120.1
Macroglossus sobrinus	PVKZ01002855.1, PVKZ01000436.1
Nilgiritragus hylocrius	PVJR01000372.1
Pipistrellus pipistrellus	PVIQ01039314.1, PVIQ01013964.1
Miniopterus schreibersii	PVJG01008891.1, PVJG01006230.1
Tadarida brasiliensis	PVIG010153414.1, PVIG010019173.1
Tragulus javanicus	PVHZ010004693.1
Scalopus aquaticus	PVIJ01000069.1, PVIJ01020978.1, PVIJ01009280.1
Mellivora capensis	PISX010000947.1, PISX010019307.1, PISX010008037.1
Pteronura brasiliensis	PJEN01011267.1
Paradoxurus hermaphroditus	PITB01026266.1, PITB01059966.1, PITB01005683.1
Spilogale gracilis	PITA01006636.1, PITA01007341.1
Suricata suricatta	PITD01000640.1

Cryptoprocta ferox	PJEU01001187.1
Helogale parvula	PJEM01000325.1
Mungos mungo	PISW01009134.1
Bos indicus	PRDE01000009.1
Giraffa tippelskirchi	LVKQ01071482.1
Rhinolophus sinicus	LVEH01000073.1
Miniopterus natalensis	LDJU01000030.1
Myotis myotis	PVIZ010005403.1, PVIZ010028134.1, PVIZ010015800.1
Lycaon pictus	SIDF01000198.1, SIDF01000354.1
Felis nigripes	PISY01019069.1
Vulpes lagopus	PISU010016330.1
Capra aegagrus	CBYH010071014.1
Tapirus indicus	PVIE01006658.1
Ceratotherium simum simum	AKZM01017598.1
Megaderma lyra	AWHB01348444.1, AWHB01348443.1, AWHB01174333.1
Eidolon helvum	AWHC01029981.1, AWHC01218502.1
Beatragus hunteri	PVKQ01021312.1, PVKQ01017688.1
Panthera onca	PISV01001604.1
Bos mutus	AGSK01075302.1
Myotis brandtii	ANKR01273868.1, ANKR01273869.1
Arctocephalus gazella	UIRR01000066.1
Pseudois nayaur	NIZD01207746.1
Axis porcinus	QQTR01093826.1
Antilocapra americana	PVKT010017748.1, PVKT010022490.1, PVKT010021272.1
Capreolus capreolus	CCMK010104759.1, CCMK012865005.1, CCMK010278719.1
Hyaena hyaena	PITC01001695.1
Okapia johnstoni	LVCL010093660.1
Capra sibirica	NIYN02075614.1
Saiga tatarica	PVIK010056808.1, PVIK010249056.1, PVIK010199988.1
Neovison vison	FNWR01000138.1
Ursus maritimus	AVOR01014285.1
Uropsilus gracilis	PVHY01011105.1, PVHY01009996.1, PVHY01036662.1, PVHY01043015.1
Hipposideros armiger	JXIK01000334.1
Elaphurus davidianus	JRFZ01051564.1
Myotis davidii	ALWT01125743.1
Acinonyx jubatus	QURD01000010.1, QURD01003229.1

Odobenus rosmarus divergens	ANOP01028105.1
Zalophus californianus	UZVU01000015.1
Ursus americanus	LZNR01003954.1
Lasiurus borealis	PVJN01073722.1, PVJN01067959.1
Puma concolor	PSOM01125930.1
Oryx gazella	RAWW01011422.1
Pteropus alecto	ALWS01011689.1
Camelus ferus	AGVR01051296.1
Eptesicus fuscus	ALEH01005956.1
Condylura cristata	AJFV01047153.1
Pantholops hodgsonii	AGTT01188813.1
Camelus bactrianus	JARL01016741.1
Camelus dromedarius	JDVD01000358.1, JDVD01000357.1
Capra hircus	XM_018061376.1
Leptonychotes weddellii	APMU01115166.1, APMU01141180.1
Moschus moschiferus	PVHU010011962.1
Diceros bicornis	PVJY010007317.1
Panthera pardus	LQGZ01015847.1, LQGZ01015848.1
Gulo gulo	CYRY02013062.1, CYRY02011280.1, CYRY02020271.1
Ammotragus lervia	NIVO01003382.1
Callorhinus ursinus	QLOG01010939.1
Neomonachus schauinslandi	NINY01007775.1
Rangifer tarandus	PVIN010004838.1
Rousettus aegyptiacus	PVIL01002740.1
Eumetopias jubatus	SBAQ01004386.1
Hippopotamus amphibius	PVJP01000741.1
Phoca vitulina	RXNX01005441.1
Mustela putorius furo	AEYP01069989.1
Ailuropoda melanoleuca	ACTA01016457.1
Bubalus bubalis	AWWX01630119.1, AWWX01532946.1, AWWX01596091.1
Pteropus vampyrus	ABRP02126915.1
Myotis lucifugus	AAPE02001462.1
Erinaceus europaeus	AMDU01193160.1, AMDU01193161.1, AMDU01193162.1
Sorex araneus	AALT02056093.1, AALT02155448.1, AALT02155449.1, AALT02155451.1
Canis lupus familiaris	PVKO01002176.1
Bos taurus	AAFC05027895.1

Felis catus	ACBE01132809.1, ACBE01132808.1
Orycteropus afer	RJWU010033725.1
Chrysochloris asiatica	AMDV01244956.1, AMDV01244955.1
Procavia capensis	PVIO010051185.1, PVIO010106105.1, PVIO010104336.1**,** PVIO010033217.1, PVIO010011627.1, PVIO010086663.1
Echinops telfairi	AAIY02209271.1
Microgale talazaci	PVJH01011807.1, PVJH01001118.1, PVJH01014246.1, PVJH01039024.1
Elephantulus edwardii	AMGZ01097263.1

Table S3. References used to construct phylogenetic tree (Appendix file 1) for ancestral sequence reconstruction.

Species placement	Reference
Tree was based primarily on this reference	M. J. Gaudry, M. Jastroch, J. R. Treberg, M. Hofreiter, J. L. A. Paijmans, J. Starrett, N. Wales, A. V. Signore, M. S. Springer, K. L. Campbell, Inactivation of thermogenic UCP1 as a historical contingency in multiple placental mammal clades. *Sci Adv* **3**, e1602878 (2017).
Ellobius lutescens; Ellobius talpinus	N. I. Abramson, V. S. Lebedev, A. S. Tesakov, A. A. Bannikova, Supraspecies relationships in the subfamily Arvicolinae (Rodentia, Cricetidae): An unexpected result of nuclear gene analysis. *Mol Biol* **43**, 834–846 (2009).
Miniopterus natalensis; Miniopterus schreibersii; Pipistrellus pipistrellus; Lasiurus borealis	I. Agnarsson, C. M. Zambrana-Torrelio, N. P. Flores-Saldana, L. J. May-Collado, A time-calibrated species-level phylogeny of bats (Chiroptera, Mammalia). *PLoS Curr* **3**, RRN1212 (2011).
Cryptoprocta ferox	I. Agnarsson, M. Kuntner, L. J. May-Collado, Dogs, cats, and kin: A molecular species-level phylogeny of Carnivora. *Mol Phylogenetics Evol* **54**, 726–745 (2010).
Tadarida brasiliensis	L. K. Ammerman, D. N. Lee, T. M. Tipps, First molecular phylogenetic insights into the evolution of free-tailed bats in the subfamily Molossinae (Molossidae, Chiroptera). *J Mammal* **93**, 12–28 (2012).
Lycaon pictus; Vulpes lagopus; Vulpes vulpes	C. Bardeleben, R. L. Moore, R. K. Wayne, A molecular phylogeny of the Canidae based on six nuclear loci. *Mol Phylogenetics Evol* **37**, 815–831 (2005).

Ammotragus lervia; Antilocapra americana; Axis porcinus; Bison bison; Bos mutus; Capra sibirica; Cervus elaphus; Giraffa tippelskirchi; Moschus moschiferus; Odocoileus hemionus; Odocoileus virginianus; Okapia johnstoni; Oryx gazella; Pseudois nayaur; Saiga tatarica; Tragulus javanicus	F. Bibi, A multi-calibrated mitochondrial phylogeny of extant Bovidae (Artiodactyla, Ruminantia) and the importance of the fossil record to systematics. *BMC Evol Bio*l **13**, 166 (2013).
Arctocephalus gazella; Callorhinus ursinus; Eumetopias jubatus; Neomonachus schauinslandi; Zalophus californianus	O. R. P. Bininda-Emonds, J. L. Gittleman, A. Purvis, Building large trees by combining phylogenetic information: a complete phylogeny of the extant Carnivora (Mammalia). *Biol Rev* **74**, 143–175 (1999).
Xerus inauris	M. D. Bryant, Phylogeny of Nearctic Sciuridae. *Am Midl Nat* **33**, 257–390 (1945).
Capromys pilorides; Dinomys branickii; Hystrix cristata; Myocastor coypus	P. H.Fabre, T. Galewski, M. K. Tilak, E. J. Douzer, Diversification of South American spiny rats (Echimyidae): a multigene phylogenetic approach. *Zool Scr* **42**, 117-134 (2013).
Ailurus fulgens; Hyaena hyaena; Paradoxurus hermaphroditus	J. J. Flynn, J. A. Finarelli, S. Zehr, J. Hsu, M. A. Nedbal, Molecular Phylogeny of the Carnivora (Mammalia): Assessing the Impact of Increased Sampling on Resolving Enigmatic Relationships. *Syst Biol* **54**, 317–337 (2005).

Hipposideros armiger; Hipposideros galeritus; Macroglossus sobrinus; Rousettus aegyptiacus	N. P. Giannini, N. B. Simmons, A phylogeny of megachiropteran bats (Mammalia: Chiroptera: Pteropodidae) based on direct optimization analysis of one nuclear and four mitochondrial genes. *Cladistics* **19**, 496–511 (2003).
Elaphurus davidianus; Rangifer tarandus	C. Gilbert, A. Ropiquet, A. Hassanin, Mitochondrial and nuclear phylogenies of Cervidae (Mammalia, Ruminantia): Systematics, morphology, and biogeography. *Mol Phylogenetics Evol* **40**, 101–117 (2006).
Urocitellus parryii	M. D. Herron, T. A. Castoe, C. L. Parkinson, Sciurid phylogeny and the paraphyly of Holarctic ground squirrels (Spermophilus). *Mol Phylogenetics Evol* **31**, 1015–1030 (2004).
Castor canadensis; Ctenodactylus gundi; Dasyprocta punctata; Glis glis; Lepus americanus; Muscardinus avellanarius; Petromus typicus; Thryonomys swinderianus	D. Huchon, O. Madsen, M. J. J. B. Sibbald, K. Ament, M. J. Stanhope, F. Catzeflis, W. W. de Jong, E. J. P. Douzery, Rodent Phylogeny and a Timescale for the Evolution of Glires: Evidence from an Extensive Taxon Sampling Using Three Nuclear Genes. *Mol Biol Evol* **19**, 1053–1065 (2002).
Craseonycteris thonglongyai	P. Hulva, I. Horáček, Craseonycteris thonglongyai (Chiroptera: Craseonycteridae) is a Rhinolophoid: Molecular Evidence from Cytochrome b. *Acta Chiropt* **4**, 107–120 (2002).
Camelus bactrianus; Camelus dromedarius	R. Ji, P. Cui, F. Ding, J. Geng, H. Gao, H. Zhang, J. Yu, S. Hu, H. Meng, Monophyletic origin of domestic bactrian camel (*Camelus bactrianus*) and its evolutionary relationship with the extant wild camel (*Camelus bactrianus ferus*). *Anim Genet* **40**, 377–382 (2009).
Pteronura brasiliensis; Taxidea taxus; Enhydra lutris; Gulo gulo; Mellivora capensis	K.-P. Koepfli, K. A. Deere, G. J. Slater, C. Begg, K. Begg, L. Grassman, M. Lucherini, G. Veron, R. K. Wayne, Multigene phylogeny of the Mustelidae: Resolving relationships, tempo and biogeographic history of a mammalian adaptive radiation. *BMC Biol* **6**, 10 (2008).

Heterohyrax brucei, Microgale talazaci	M. Kuntner, L. J. May-Collado, I. Agnarsson, Phylogeny and conservation priorities of afrotherian mammals (Afrotheria, Mammalia). *Zool Scr* **40**, 1–15 (2011).
Panthera onca; Panthera tigris	W. Lei, W. XiaoBing, L. Zhu, Z. Jiang, Mitogenomic analysis of the genus Panthera. *Sci China Life Sci* **54**, 917–930 (2011).
Mus caroli; Mus pahari; Mus spicilegus; Mus spretus	B. L. Lundrigan, S. A. Jansa, P. K. Tucker, Phylogenetic Relationships in the Genus Mus, Based on Paternally, Maternally, and Biparentally Inherited Characters. *Syst Biol* **51**, 410–431 (2002).
Beatragus hunteri	C. A. Matthee, S. K. Davis, Molecular Insights into the Evolution of the Family Bovidae: A Nuclear DNA Perspective. *Mol Biol Evol* **18**, 1220–1230 (2001).
Vombatus ursinus	L. J. May-Collado, C. W. Kilpatrick, I. Agnarsson, Mammals from 'down under': a multi-gene species-level phylogeny of marsupial mammals (Mammalia, Metatheria). *PeerJ* **3**, e805 (2015).
Ursus americanus; Ursus arctos	M. Pagès, S. Calvignac, C. Klein, M. Paris, S. Hughes, C. Hänni, Combined analysis of fourteen nuclear genes refines the Ursidae phylogeny. *Mol Phylogenetics Evol* **47**, 73–83 (2008).
Helogale parvula; Mungos mungo; Suricata suricatta	M.-L. Patou, P. A. Mclenachan, C. G. Morley, A. Couloux, A. P. Jennings, G. Veron, Molecular phylogeny of the Herpestidae (Mammalia, Carnivora) with a special emphasis on the Asian Herpestes. *Mol Phylogenetics Evol* **53**, 69–80 (2009).

Alouatta palliata; Aotus nancymaae; Ateles geoffroyi; Cebus albifrons; Cebus capucinus; Cercopithecus neglectus; Cheirogaleus medius; Erythrocebus patas; Eulemur fulvus; Indri indri; Lemur catta; Macaca fuscata; Mandrillus sphinx; Mirza coquereli; Nycticebus coucang; Piliocolobus tephrosceles; Pithecia pithecia; Plecturocebus donacophilus; Prolemur simus; Pygathrix nemaeus; Saguinus imperator; Saimiri boliviensis boliviensis; Semnopithecus entellus; Theropithecus gelada	P. Perelman, W. E. Johnson, C. Roos, H. N. Seuánez, J. E. Horvath, M. A. M. Moreira, B. Kessing, J. Pontius, M. Roelke, Y. Rumpler, M. P. C. Schneider, A. Silva, S. J. O'Brien, J. Pecon-Slattery, A Molecular Phylogeny of Living Primates. *PLOS Genet* **7**, e1001342 (2011).
Tupaia chinensis; Tupaia tana	T. E. Roberts, H. C. Lanier, E. J. Sargis, L. E. Olson, Molecular phylogeny of treeshrews (Mammalia: Scandentia) and the timescale of diversification in Southeast Asia. *Mol Phylogenetics Evol* **60**, 358–372 (2011).
Cuniculus paca; Dolichotis patagonum; Hydrochoerus hydrochaeris	D. L. Rowe, R. L. Honeycutt, Phylogenetic Relationships, Ecological Correlates, and Molecular Evolution Within the Cavioidea (Mammalia, Rodentia). *Mol Biol Evol* **19**, 263–277 (2002).
Perognathus longimembris	J.M. Ryan, Comparative myology and phylogenetic systematics of the Heteromyidae (Mammalia, Rodentia). *Misc Publ Mus Zool Univ Mich* **176**, 1-103 (1989).

Cavia tschudii	A. Spotorno, P. Valladares, J. Marin, H. Zeballos, Molecular diversity among domestic guinea-pigs (*Cavia porcellus*) and their close phylogenetic relationship with the Andean wild species *Cavia tschudii*. *Rev Chil Hist Nat* **77**, 243-250 (2004).
Myotis myotis	B. Stadelmann, D. S. Jacobs, C. Schoeman, M. Ruedi, Phylogeny of African Myotis bats (Chiroptera, Vespertilionidae) inferred from cytochrome b sequences. *Acta Chiropt* **6**, 177–192 (2004).
Marmota flaviventris; Marmota himalayana; Peromyscus maniculatus; Sigmodon hispidus; Zapus hudsonius; Acomys cahirinus; Allactaga bullata; Cricetomys gambianus; Graphiurus murinus	S. J. Steppan, M. R. Akhverdyan, E. A. Lyapunova, D. G. Fraser, N. N. Vorontsov, R. S. Hoffmann, M. J. Braun, Molecular Phylogeny of the Marmots (Rodentia: Sciuridae): Tests of Evolutionary and Biogeographic Hypotheses. *Syst Biol* **48**, 715–734 (1999).
Aplodontia rufa	S. J. Steppan, R. M. Adkins, J. Anderson. Phylogeny and divergence-date estimates of rapid radiations in muroid rodents based on multiple nuclear genes. *Syst Biol* **53**, 533-553 (2004).
Neotoma lepida; Ondatra zibethicus; Onychomys torridus; Psammomys obesus; Rhizomys pruinosus; Grammomys surdaster; Meriones unguiculatus	S. J. Steppan, J. J. Schenk, Muroid rodent phylogenetics: 900-species tree reveals increasing diversification rates. *PloS one* **12**, e0183070 (2017).
Ctenomys sociabilis; Octomys mimax; Tympanoctomys barrerae	D. H. Verzi, Phylogenetic position of Abalosia and the evolution of the extant Octodontinae (Rodentia, Caviomorpha, Octodontidae). *Acta Theriol* **46**, 243–268 (2001).

Scalopus aquaticus; Uropsilus gracilis	H. P. Whidden, Comparative Myology of Moles and the Phylogeny of the Talpidae (Mammalia, Lipotyphla). *Am Mus Novit* **2000**, 1–53 (2000).
Spilogale gracilis	L. Yu, D. Peng, J. Liu, P. Luan, L. Liang, H. Lee, M. Lee, O. A. Ryder, Y. Zhang, On the phylogeny of Mustelidae subfamilies: analysis of seventeen nuclear non-coding loci and mitochondrial complete genomes. *BMC Evol Biol* **11**, 92 (2011).

Table S4 Accession numbers of data-mined UCP1 containing contigs of virtually translated amino acids sequences in Figure S7.

Species name	Common name	Accession
Monodelphis domestica	Gray short-tailed opossum	OP589293.1
Thylacinus cynocephalus	Tasmanian wolf	VAHE03000006.1
Macropus fuliginosus	Western grey kangaroo	JAQMYV010019862.1
Vombatus ursinus	Common wombat	JAQQSX010000006.1
Trichosurus vulpecula	Common brushtail possum	JAANDF010001260.1
Sarcophilus harrisii	Tasmanian devil	AEFK01215941.1; AEFK01119955.1
Dromiciops gliroides	Monito del monte	JAHYBS010006255.1
Bettongia penicillata	Brush-tailed bettong	JAJHZJ010000494.1
Dasyurus viverrinus	Eastern quoll	JAJAFV010000005.1
Pseudocheirus occidentalis	Western ringtail possum	JAQQSW010000009.1
Antechinus flavipes	Yellow-footed antechinus	JADWMD010000006.1
Gymnobelideus leadbeateri	Leadbeater's possum	WOXC01009792.1
Macropus giganteus	Eastern grey kangaroo	JAQQTA010000003.1
Myrmecobius fasciatus	Numbat	JAJPUD010000169.1
Lagorchestes hirsutus	Rufous hare-wallaby	JAPYYB010000007.1
Ornithorhynchus anatinus	Platypus	PTTO01001633.1
Tachyglossus aculeatus	Short-beaked echidna	JADRJF010000464.1